

# Kadanoff-Baym Equations with Non-Gaussian Initial Conditions: The Equilibrium Limit

Mathias Garny\*

*Max-Planck-Institut für Kernphysik  
Saupfercheckweg 1, 69117 Heidelberg, Germany*

Markus Michael Müller†

*Leibniz-Rechenzentrum,  
Boltzmannstraße 1, 85748 Garching, Germany*

(Dated: December 2, 2018)

The nonequilibrium dynamics of quantum fields is an initial-value problem, which can be described by Kadanoff-Baym equations. Typically, and in particular when numerical solutions are demanded, these Kadanoff-Baym equations are restricted to Gaussian initial states. However, physical initial states are non-Gaussian correlated initial states. In particular, renormalizability requires the initial state to feature  $n$ -point correlations that asymptotically agree with the vacuum correlations at short distances for  $n \leq 4$ . In order to identify physical nonequilibrium initial states, it is therefore a precondition to describe the vacuum correlations of the interacting theory within the nonequilibrium framework. In this paper, Kadanoff-Baym equations for non-Gaussian correlated initial states describing vacuum and thermal equilibrium are derived from the 2PI effective action. A diagrammatic method for the explicit construction of vacuum and thermal initial correlations from the 2PI effective action is provided. We present numerical solutions of Kadanoff-Baym equations for a real scalar  $\Phi^4$  quantum field theory which take the initial 4-point correlation as the leading non-Gaussian correction into account. We find that this minimal non-Gaussian initial condition yields an approximation to the complete equilibrium initial state that is quantitatively and qualitatively significantly improved as compared to Gaussian initial states.

PACS numbers: 11.10.Wx, 98.80.Cq, 12.38.Mh

## I. INTRODUCTION

Nonequilibrium processes within astro-particle and high-energy physics, like reheating after inflation, baryogenesis, or relativistic heavy ion collisions, are typically described by classical or semi-classical equations. These include Boltzmann equations, hydrodynamic transport equations or effective equations of motion for a coherent scalar field expectation value [1–3]. The semi-classical treatment provides the possibility to relate fundamental parameters of the underlying theory with model predictions. Although inflation and baryogenesis occur at extremely high energies, key observables like the baryon asymmetry and the spectral index are subject to experimental verification, for example by measurements of the cosmic microwave background radiation [4]. Therefore it is of great importance to assess the reliability of the underlying semi-classical approximations. This can be achieved by a comparison with a completely quantum field theoretical treatment.

In recent years it has been demonstrated that the time evolution of relativistic scalar and fermionic quantum fields far from equilibrium can be described based on

first principles by Kadanoff-Baym equations [5–9]. These equations for the complete one- and two-point correlation functions can be obtained from the stationarity conditions of the 2PI effective action [10] defined on the closed real-time contour [11–13]. The advantages of this approach are manifold: First, its conceptual simplicity is very attractive. The only assumption entering the derivation of Kadanoff-Baym equations is the truncation of the so-called 2PI functional, which amounts to a controlled approximation in the coupling constant or the inverse number of field degrees of freedom for specific quantum field theories [6]. Furthermore, Kadanoff-Baym equations inherently incorporate typical quantum (e.g. off-shell) effects as well as ‘classical’ (e.g. on-shell) effects in a unified manner, and can be applied even to systems far from equilibrium. Accordingly, they are very versatile and can be employed both to assess the validity of conventional semi-classical approximations (e.g. for baryogenesis and leptogenesis), and in situations where a single effective description does not exist (e.g. for (p)reheating by inflaton decay and subsequent thermalization) [14, 15].

It has been shown that numerical solutions of Kadanoff-Baym equations not only provide a description of the quantum thermalization process of relativistic quantum fields for closed systems [5, 16, 17], but also feature a separation of time-scales between kinetic and chemical equilibration (prethermalization) [18]. Furthermore, they

---

\*Electronic address: [Mathias.Garny@mpi-hd.mpg.de](mailto:Mathias.Garny@mpi-hd.mpg.de)

†Electronic address: [Markus.Michael.Mueller@lrz.de](mailto:Markus.Michael.Mueller@lrz.de)

have been compared to semi-classical transport equations for bosonic and fermionic systems [7, 9, 19, 20] (see also Refs. [21–25] for the non-relativistic case). Moreover, Kadanoff-Baym equations can describe the decay of a coherent, oscillating scalar field expectation value under conditions where parametric resonance occurs [16], and have also been investigated in curved space-time [26, 27].

These successes of the 2PI effective action and Kadanoff-Baym equations in the area of nonequilibrium quantum field theory make it worthwhile and, in view of realistic applications, necessary to answer remaining conceptual questions, like renormalization. The renormalization of the 2PI effective action in vacuum and at finite temperature has been established recently [28–32]. It has been shown that the vacuum counterterms are also sufficient at finite temperature. In order to extend this proof to nonequilibrium situations, it is necessary to identify initial states that are themselves free of divergences. In particular, this requires that the correlation functions characterizing these *physical* initial states are rendered finite by the vacuum counterterms.

Typically, Kadanoff-Baym equations are solved for Gaussian initial states. All connected  $n$ -point correlation functions with  $n > 2$  vanish for Gaussian initial states by definition. However, in vacuum and at finite temperature the 3- and 4-point correlation functions carry overall divergences that are cancelled by corresponding vacuum counterterms. Thus Gaussian initial states lead to an unbalanced divergence at the initial time [33]. In order to overcome this shortcoming, physical initial states have to carry non-Gaussian initial 3- and 4-point correlation functions that differ from the vacuum correlations at most by a finite amount.

In order to be able to identify physical initial states, it is therefore a precondition to be able to describe vacuum and thermal equilibrium within the standard framework of nonequilibrium quantum field theory, i.e. on the closed real-time path with finite initial time  $t_{init} \equiv 0$ . Apart from the question of renormalization it is also a matter of principle that vacuum and thermal equilibrium should be accessible within nonequilibrium field theory as special cases by choosing the initial state appropriately.

In this work, Kadanoff-Baym equations for non-Gaussian correlated initial states describing vacuum and thermal equilibrium are derived from the 2PI effective action formulated on the closed real-time path with finite initial time. For that purpose, we propose a diagrammatic method for the explicit construction of vacuum and thermal initial correlations that is applicable to nonperturbative 2PI approximations.

There exist several techniques to describe non-Gaussian correlated initial states. These can be divided into two categories: Either, the correlations are generated by modifying the closed real-time path  $\mathcal{C}$ , or the initial state is explicitly described by its density matrix  $\rho$ . We shall refer to these as *implicit* and *explicit* techniques, respectively. The implicit techniques include the so-called imaginary-time stepping [13, 21, 22], where an imaginary

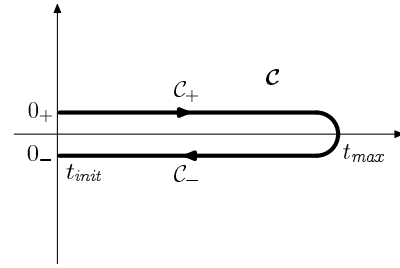


FIG. 1: Closed real-time path  $\mathcal{C}$ . This time path was invented by Schwinger [11] and applied to non-equilibrium problems by Keldysh [12]. In order to avoid the doubling of the degrees of freedom, we use the form presented in Ref. [13].

branch is added to the contour  $\mathcal{C}$ , similar to the description of thermal field theory [34–36]. Another possibility is to extend the closed real-time contour  $\mathcal{C}$  over the complete real axis, such that it runs from  $-\infty$  to  $+\infty$ , and back to  $-\infty$ . The correlated initial state is then generated by including an external two-point source  $K(x, y)$ , that is switched off at the ‘initial’ time [33].

For the explicit technique, the density matrix  $\rho$  of the initial state is parameterized by initial  $n$ -point correlation functions  $\alpha_n(x_1, \dots, x_n)$  [37, 38]. These appear in the form of non-local effective  $n$ -point vertices in the 2PI effective action. When deriving Kadanoff-Baym equations, these inherit the contributions from non-Gaussian initial correlations.

The advantage of the implicit techniques is that the equilibrium limit can be approached without any additional work. However, due to the implicit preparation of the initial state, the freedom and the control in choosing the initial state is restricted. The advantage of the explicit technique is that the resulting Kadanoff-Baym equations are very similar to the Gaussian case. Furthermore, the explicit approach provides a maximal degree of freedom for specifying the initial state.

The renormalization of Kadanoff-Baym equations has recently been discussed based on the implicit technique involving an external two-point source [33]. In this work, we use the explicit technique. Thus, the methods developed in this paper provide a complementary framework for addressing the issue of renormalization.

In section II, we derive Kadanoff-Baym equations for non-Gaussian initial states from the corresponding 2PI effective action using the explicit technique. In section III, we provide techniques for calculating the non-Gaussian initial correlations  $\alpha_n^{th}(x_1, \dots, x_n)$  for a thermal initial state  $\rho_{th}$  within perturbation theory. These techniques are generalized to the nonperturbative 2PI case in section IV. In section V, Kadanoff-Baym equations for a thermal initial state are derived by combining the results from sections II and IV. In section VI, we compare numerical solutions of Kadanoff-Baym equations for two initial states that are approximations to the thermal initial state. One of them is Gaussian, while the other also includes the leading non-Gaussian initial correlation. The

appendices A and B contain additional material helpful for sections III and IV, respectively.

## II. EFFECTIVE ACTION AND KADANOFF-BAYM EQUATIONS

### A. Gaussian Initial States

In this subsection, we start from the classical action for a real scalar quantum field with a quartic self interaction

$$S[\phi] = \int d^4x \left( \frac{1}{2}(\partial\phi)^2 - \frac{1}{2}m^2\phi^2 - \frac{\lambda}{4!}\phi^4 \right), \quad (1)$$

and review the basic elements of the derivation of the 2PI effective action and the Kadanoff-Baym equations for the case of a Gaussian initial state. In the following subsections, we can then easily expose the differences, which arise for a non-Gaussian initial state.

The Schwinger-Keldysh propagator is defined by

$$G(x, y) = \langle T_{\mathcal{C}} \Phi(x)\Phi(y) \rangle - \langle \Phi(x) \rangle \langle \Phi(y) \rangle, \quad (2)$$

where  $T_{\mathcal{C}}$  denotes the time-ordering operator along the closed real-time path  $\mathcal{C}$  shown in figure 1 [11–13]. The Schwinger-Keldysh propagator can be obtained by functional differentiation from the generating functional for correlation functions formulated on the closed real-time path. The generating functional in the presence of a local external source  $J(x)$  and a bilocal external source  $K(x, y)$  is given by [38]

$$\begin{aligned} Z_{\rho}[J, K] &= \int \mathcal{D}\varphi(x) \langle \varphi_+ | \rho | \varphi_- \rangle \\ &\times \exp \left( iS[\varphi] + iJ\varphi + \frac{i}{2}\varphi K\varphi \right), \end{aligned} \quad (3)$$

where a matrix-vector notation has been used for the space-time integrals in the exponential function<sup>1</sup>, and  $|\varphi_{\pm}\rangle$  are the quantum states corresponding to the field configurations  $\varphi_{\pm}(\mathbf{x}) = \varphi(0_{\pm}, \mathbf{x})$ . The information about the initial state enters via the matrix element of the density matrix  $\rho$ , which is known only at the initial time  $t = t_{init} \equiv 0$ .

A Gaussian initial state is an initial state for which all connected  $n$ -point correlation functions with  $n \geq 3$  vanish at the initial time. The density matrix element for a Gaussian initial state can be parameterized by

$$\langle \varphi_+ | \rho | \varphi_- \rangle = \exp \left( i\alpha_0 + i\alpha_1\varphi + \frac{i}{2}\varphi\alpha_2\varphi \right). \quad (4)$$

<sup>1</sup> Throughout this work, the compact notation of Ref. [13] is used for the contour integrals over the closed real-time path, for example  $J\varphi \equiv \int_{\mathcal{C}} d^4x J(x)\varphi(x) = \int d^4x [J_+(x)\varphi_+(x) - J_-(x)\varphi_-(x)]$ .

Therefore, in the Gaussian case, the contribution of the density matrix to the generating functional (3) can be absorbed into the external sources,  $J + \alpha_1 \rightarrow J$  and  $K + \alpha_2 \rightarrow K$ .

The 2PI effective action  $\Gamma[\phi, G]$  is the double Legendre transform of the generating functional (3) with respect to the external sources. For a Gaussian initial state, the generating functional has the same structure as the generating functional in vacuum, except that all time-integrations are performed over the closed real-time path. Consequently, for a Gaussian initial state the 2PI effective action can be parameterized in the form [10]

$$\begin{aligned} \Gamma[\phi, G] &= S[\phi] + \frac{i}{2}\text{Tr} \log_{\mathcal{C}} [G^{-1}] \\ &+ \frac{i}{2}\text{Tr}_{\mathcal{C}} [\mathcal{G}_0^{-1}G] + \Gamma_2[\phi, G], \end{aligned} \quad (5)$$

where  $\mathcal{G}_0^{-1}$  is the inverse classical Schwinger-Keldysh propagator and  $i\Gamma_2[\phi, G]$  is the sum of all 2PI Feynman diagrams without any external legs, where internal lines represent the complete Schwinger-Keldysh propagator  $G(x, y)$ . The vertices of the diagrams contained in  $i\Gamma_2[\phi, G]$  are given by the third and fourth functional derivatives of the classical action  $S[\phi]$  [10]. Eventually, the Kadanoff-Baym equations

$$\begin{aligned} (\square_x + M^2(x)) G_F(x, y) &= \int_0^{y^0} d^4z \Pi_F(x, z) G_{\rho}(z, y) \\ &- \int_0^{x^0} d^4z \Pi_{\rho}(x, z) G_F(z, y), \quad (6) \\ (\square_x + M^2(x)) G_{\rho}(x, y) &= \int_{x_0}^{y^0} d^4z \Pi_{\rho}(x, z) G_{\rho}(z, y), \end{aligned}$$

follow from the stationarity condition of the 2PI effective action. Here, we use the notation of Ref. [9].

### B. Non-Gaussian Initial States

In the remainder of this section, Kadanoff-Baym equations are derived that can describe systems characterized by a general non-Gaussian initial state [37–39]. For that purpose, we extend the derivation of the previous subsection using a generalization of the Gaussian density matrix (4). In general, the matrix element of the density matrix  $\rho$  is an arbitrary functional of the field configurations  $\varphi_+(\mathbf{x})$  and  $\varphi_-(\mathbf{x})$ , which can be written as [38]

$$\langle \varphi_+ | \rho | \varphi_- \rangle = \exp(iF[\varphi]). \quad (7)$$

While for a Gaussian initial state  $F[\varphi]$  is a quadratic functional of the field, for a general non-Gaussian initial

state it may be Taylor expanded in the form [38]

$$F[\varphi] = \sum_{n=0}^{\infty} \frac{1}{n!} \int_{\mathcal{C}} d^4x_1 \dots d^4x_n \alpha_n(x_1, \dots, x_n) \times \varphi(x_1) \dots \varphi(x_n). \quad (8)$$

By definition  $F[\varphi]$  depends only on the field configuration evaluated at the boundaries of the time contour. Consequently, the kernels  $\alpha_n(x_1, \dots, x_n)$  are nonzero only if all their time arguments lie on the boundaries of the time contour. With the notation  $\delta_+(t) = \delta_{\mathcal{C}}(t - 0_+)$  and  $\delta_-(t) = \delta_{\mathcal{C}}(t - 0_-)$ , they can be written in the form

$$\alpha_n(x_1, \dots, x_n) = \alpha_n^{\epsilon_1, \dots, \epsilon_n}(\mathbf{x}_1, \dots, \mathbf{x}_n) \times \delta_{\epsilon_1}(x_1^0) \dots \delta_{\epsilon_n}(x_n^0), \quad (9)$$

where summation over  $\epsilon_j \in \{+, -\}$  is implied. In this way, the explicit dependence of the functional  $F[\varphi]$  on the field configurations  $\varphi_+(\mathbf{x})$  and  $\varphi_-(\mathbf{x})$  may be recovered,

$$F[\varphi] = \alpha_0 + \int d^3x \alpha_1^{\epsilon}(\mathbf{x}) \varphi_{\epsilon}(\mathbf{x}) + \dots$$

The set of all kernels  $\alpha_n$  with  $n \geq 0$  encodes the complete information about the density matrix characterizing the initial state. Not all the kernels are independent. The Hermiticity of the density matrix,  $\rho = \rho^\dagger$ , implies that

$$i\alpha_n^{\epsilon_1, \dots, \epsilon_n}(\mathbf{x}_1, \dots, \mathbf{x}_n) = \left( i\alpha_n^{(-\epsilon_1), \dots, (-\epsilon_n)}(\mathbf{x}_1, \dots, \mathbf{x}_n) \right)^*.$$

If the initial state is invariant under some symmetries, there are further constraints. For example, for an initial state which is invariant under the  $Z_2$ -symmetry  $\Phi \rightarrow -\Phi$ , all kernels  $\alpha_n(x_1, \dots, x_n)$  with odd  $n$  vanish. If the initial state is homogeneous in space, the initial correlations  $\alpha_n(x_1, \dots, x_n)$  are invariant under space-translations  $\mathbf{x}_i \rightarrow \mathbf{x}_i + \mathbf{a}$  of all arguments for any real three-vector  $\mathbf{a}$ , and can conveniently be expressed in spatial momentum space,

$$\begin{aligned} & \alpha_n^{\epsilon_1, \dots, \epsilon_n}(\mathbf{x}_1, \dots, \mathbf{x}_n) \\ &= \int \frac{d^3k_1}{(2\pi)^3} \dots \int \frac{d^3k_n}{(2\pi)^3} \exp\left(i \sum_j \mathbf{k}_j \mathbf{x}_j\right) \\ & \times (2\pi)^3 \delta^3(\mathbf{k}_1 + \dots + \mathbf{k}_n) \alpha_n^{\epsilon_1, \dots, \epsilon_n}(\mathbf{k}_1, \dots, \mathbf{k}_n). \end{aligned}$$

Summarizing, the generating functional reads

$$Z_\rho[J, K] = \int \mathcal{D}\varphi \exp\left(iS[\varphi] + iJ\varphi + \frac{i}{2} \varphi K \varphi + iF_3[\varphi]\right), \quad (10)$$

where the kernels  $\alpha_0$ ,  $\alpha_1$  and  $\alpha_2$  have been absorbed into the measure  $\mathcal{D}\varphi$  and into the sources  $J$  and  $K$ , respectively. The functional  $F_3[\varphi] \equiv F_3[\varphi; \alpha_3, \alpha_4, \dots]$  contains the contributions of third, fourth and higher orders of the Taylor expansion (8) and vanishes for a Gaussian initial state.

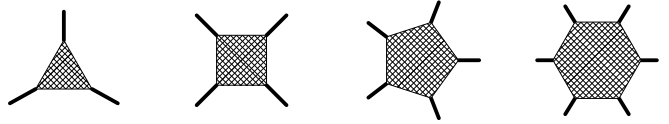


FIG. 2: Non-local effective vertices  $i\bar{\alpha}_n(x_1, \dots, x_n)$  connecting  $n$  lines for  $n = 3, 4, 5, 6$  encoding the non-Gaussian three-, four-, five-, six-, ...-point correlations of the initial state.

### C. 2PI Effective Action for Non-Gaussian Initial States

According to eq. (10), the 2PI effective action in the presence of non-Gaussian correlations is obtained from the standard parameterization [10] of the 2PI effective action applied to a theory described by the modified classical action  $\tilde{S}[\phi] \equiv S[\phi] + F_3[\phi]$ ,

$$\begin{aligned} \Gamma[\phi, G] &= \tilde{S}[\phi] + \frac{i}{2} \text{Tr} \log_{\mathcal{C}} [G^{-1}] \\ &+ \frac{i}{2} \text{Tr}_{\mathcal{C}} \left[ \tilde{G}_0^{-1} G \right] + \tilde{\Gamma}_2[\phi, G] \\ &\equiv \Gamma_G[\phi, G] + \Gamma_{nG}[\phi, G], \end{aligned} \quad (11)$$

where  $i\tilde{G}_0^{-1}(x, y) \equiv \delta^2 \tilde{S}[\phi] / \delta\phi(x) \delta\phi(y)$ . The Gaussian part  $\Gamma_G[\phi, G]$  coincides with the right-hand side of eq. (5), and the non-Gaussian part is given by

$$\Gamma_{nG}[\phi, G] = F_3[\phi] + \frac{1}{2} \text{Tr}_{\mathcal{C}} \left[ \frac{\delta^2 F_3}{\delta\phi \delta\phi} G \right] + \Gamma_{2, nG}[\phi, G],$$

where

$$\Gamma_{2, nG}[\phi, G] \equiv \tilde{\Gamma}_2[\phi, G] - \Gamma_2[\phi, G].$$

The modified 2PI functional  $i\tilde{\Gamma}_2[\phi, G]$  is equal to the sum of all 2PI Feynman diagrams without any external legs, where internal lines represent the complete propagator  $G(x, y)$  and where vertices are given by the functional derivatives of the modified classical action  $\tilde{S}[\phi] = S[\phi] + F_3[\phi]$ . The contribution from the classical action  $S[\phi]$  leads to the classical local three- and four-point vertices. Additionally, the contribution from the functional  $F_3[\phi]$  leads to effective non-local vertices, which contain the non-Gaussian initial  $n$ -point correlations with  $n \geq 3$  (see figure 2),

$$i \frac{\delta^n F_3[\phi]}{\delta\phi(x_1) \dots \delta\phi(x_n)} \equiv i\bar{\alpha}_n(x_1, \dots, x_n). \quad (12)$$

These effective  $n$ -point vertices are only supported at the initial time, and can be parameterized analogously to eq. (9). For a  $Z_2$ -symmetric initial state, the field expectation value vanishes,  $\phi(x) = 0$ , such that  $\bar{\alpha}_n(x_1, \dots, x_n) = \alpha_n(x_1, \dots, x_n)$ . The contribution of these effective non-local vertices is most important close to the initial time. For example, a non-zero four-point source  $\alpha_4(x_1, \dots, x_4)$  leads to a non-vanishing value of

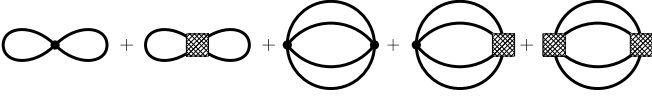


FIG. 3: Diagrams contributing to the three-loop truncation of the 2PI effective action in the symmetric phase (setting-sun approximation) in the presence of an effective non-local four-point vertex.

the connected four-point correlation function at the initial time, which is impossible for a Gaussian initial state.

Note that those 2PI diagrams which contain exclusively the classical vertices by definition contribute to the functional  $i\Gamma_2[\phi, G]$ . Therefore, the diagrams contributing to the non-Gaussian part  $i\Gamma_{2, nG}[\phi, G]$  contain at least one effective vertex from eq. (12).

In section VI we study the numerical solution of Kadanoff-Baym equations for a  $Z_2$ -symmetric non-Gaussian initial state with a non-zero initial 4-point correlation. In this case the 2PI functional  $\tilde{\Gamma}_2$  reads in “naïve”<sup>2</sup> three-loop approximation (see figure 3)

$$\begin{aligned} i\tilde{\Gamma}_2[G] &= \frac{1}{8} \int_{\mathcal{C}} d^4 x_{1234} \left[ -i\lambda\delta_{12}\delta_{23}\delta_{34} + i\alpha_{1234} \right] G_{12}G_{34} \\ &+ \frac{1}{48} \int_{\mathcal{C}} d^4 x_{1\dots 8} \left[ -i\lambda\delta_{12}\delta_{23}\delta_{34} + i\alpha_{1234} \right] \\ &\times G_{15}G_{26}G_{37}G_{48} \left[ -i\lambda\delta_{56}\delta_{57}\delta_{58} + i\alpha_{5678} \right], \end{aligned} \quad (13)$$

where  $G_{12} = G(x_1, x_2)$  and  $\alpha_{1234} = \alpha_4(x_1, x_2, x_3, x_4)$ . Note that the contribution to the mixed ‘basketball’ diagram in the second and third line with one classical and one effective vertex appears twice, which accounts for the symmetry factor  $1/24$ .

#### D. Self-Energy for Non-Gaussian Initial States

The equation of motion for the complete propagator obtained from eq. (11) reads

$$G^{-1}(x, y) = \mathcal{G}_0^{-1}(x, y) - \Pi(x, y) - i\bar{\alpha}_2(x, y), \quad (14)$$

where  $\bar{\alpha}_2 = \alpha_2 + \delta^2 F_3[\phi]/\delta\phi\delta\phi$  and the complete self-energy is given by

$$\begin{aligned} \Pi(x, y) &= \frac{2i\delta\tilde{\Gamma}_2[\phi, G]}{\delta G(y, x)} \\ &= \frac{2i\delta\Gamma_2[\phi, G]}{\delta G(y, x)} + \frac{2i\delta\Gamma_{2, nG}[\phi, G]}{\delta G(y, x)} \\ &\equiv \Pi^G(x, y) + \Pi^{nG}(x, y), \end{aligned} \quad (15)$$

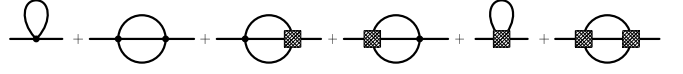


FIG. 4: Diagrams contributing to the self-energy  $\Pi(x, y)$  in setting-sun approximation in the presence of an effective non-local four-point vertex. From left to right, the diagrams contribute to  $\Pi_{loc}$ ,  $\Pi_{non-loc}^G$ ,  $\Pi_{\lambda\alpha}$ ,  $\Pi_{\alpha\lambda}$ , and the last two both contribute to  $\Pi_{\alpha\alpha}$ .

where  $\Pi^G$  contains the contributions to the self energy, which are also present for a Gaussian initial state, and the non-Gaussian part  $\Pi^{nG}$  contains diagrams with at least one non-local effective vertex. They can be further decomposed as

$$\begin{aligned} \Pi^G(x, y) &= -i\Pi_{loc}(x)\delta_{\mathcal{C}}(x-y) + \Pi_{non-loc}^G(x, y), \\ \Pi^{nG}(x, y) &= i\Pi_{surface}^{nG}(x, y) + \Pi_{non-loc}^{nG}(x, y). \end{aligned} \quad (16)$$

The non-Gaussian non-local part  $\Pi_{non-loc}^{nG}(x, y)$  contains diagrams where both external lines are attached to a standard vertex. The non-Gaussian ‘surface’ part  $i\Pi_{surface}^{nG}(x, y)$  contains diagrams where at least one external line is attached to a non-local effective vertex. Thus, the surface part is supported only at the initial time surface where  $x^0 = 0$  or  $y^0 = 0$ . In general, such contributions can arise in the following ways:

1. From diagrams where both external lines are connected to an effective non-local vertex as given in eq. (12). They are supported at  $x^0 = y^0 = 0$ .
2. From diagrams where one of the two external lines is connected to an effective non-local vertex, while the other one is connected to a classical local vertex. They are supported at  $x^0 = 0, y^0 \geq 0$  or vice-versa.
3. Via the contribution  $i\bar{\alpha}_2(x, y)$  of the initial two-point source which is supported at  $x^0 = y^0 = 0$ . This is the *only* Gaussian surface-contribution.

Accordingly, the contributions to the self-energy which are supported at the initial time surface can be further decomposed as

$$\begin{aligned} \Pi_{surface}(x, y) &= \Pi_{surface}^{nG}(x, y) + \bar{\alpha}_2(x, y) \\ &\equiv \Pi_{\alpha\alpha}(x, y) + \Pi_{\lambda\alpha}(x, y) + \Pi_{\alpha\lambda}(x, y), \end{aligned}$$

where

$$\begin{aligned} \Pi_{\alpha\alpha}(x, y) &= \delta_{\epsilon_1}(x^0)\Pi_{\alpha\alpha}^{\epsilon_1, \epsilon_2}(\mathbf{x}, \mathbf{y})\delta_{\epsilon_2}(y^0), \\ \Pi_{\lambda\alpha}(x, y) &= \Pi_{\lambda\alpha}^{\epsilon}(x^0, \mathbf{x}, \mathbf{y})\delta_{\epsilon}(y^0), \\ \Pi_{\alpha\lambda}(x, y) &= \delta_{\epsilon}(x^0)\Pi_{\alpha\lambda}^{\epsilon}(\mathbf{x}, \mathbf{y}^0, \mathbf{y}) = \Pi_{\lambda\alpha}(y, x). \end{aligned} \quad (17)$$

$\Pi_{\alpha\alpha}$  contains all contributions of type (1.) and (3.). Diagrams of type (2.) contribute to  $\Pi_{\lambda\alpha}$  or  $\Pi_{\alpha\lambda}$  depending which external line is attached to the effective non-local vertex and which to the classical local vertex. For all diagrams contributing to  $\Pi_{\lambda\alpha}$  the left line is connected to the classical four- or three-point vertex. The non-local

<sup>2</sup> This means that non-local effective vertices do not affect the counting of loops.

part of the self-energy can be split into statistical and spectral components, similarly to the Gaussian case,

$$\begin{aligned}\Pi_{non-loc}(x, y) &\equiv \Pi_{non-loc}^G(x, y) + \Pi_{non-loc}^{nG}(x, y) \quad (18) \\ &\equiv \Pi_F(x, y) - \frac{i}{2} \text{sign}_{\mathcal{C}}(x^0 - y^0) \Pi_{\rho}(x, y).\end{aligned}$$

The local part of the self-energy is identical to the Gaussian case and is included in the effective time-dependent mass term  $M^2(x) = m^2 + \Pi_{loc}(x)$ .

For the setting-sun approximation from eq. (13), the self-energy is given by (see figure 4)

$$\begin{aligned}\Pi_{non-loc}^G(x, y) &= \frac{(-i\lambda)^2}{6} G(x, y)^3, \\ \Pi_{non-loc}^{nG}(x, y) &= 0,\end{aligned}$$

$$\begin{aligned}i\Pi_{\alpha\alpha}(x, y) &= i\alpha_2(x, y) + \frac{1}{2} \int d^4x_{34} i\alpha_{xy34} G_{34} \\ &\quad + \frac{1}{6} \int d^4x_{2..7} i\alpha_{x234} G_{25} G_{36} G_{47} i\alpha_{567y}, \\ i\Pi_{\lambda\alpha}(x, y) &= \frac{-i\lambda}{6} \int d^4x_{123} G_{x1} G_{x2} G_{x3} i\alpha_{123y},\end{aligned}$$

$$i\Pi_{\alpha\lambda}(x, y) = \frac{-i\lambda}{6} \int d^4x_{234} i\alpha_{x234} G_{2y} G_{3y} G_{4y}.$$

### E. Kadanoff-Baym Equations for Non-Gaussian Initial States

Convoluting eq. (14) with the complete propagator yields

$$\begin{aligned}(\square_x + M^2(x)) G(x, y) &= -i\delta_{\mathcal{C}}(x - y) \quad (19) \\ -i \int_{\mathcal{C}} d^4z [\Pi_{non-loc}(x, z) + i\Pi_{\lambda\alpha}(x, z)] G(z, y).\end{aligned}$$

The second line follows from using the parameterization (16) of the self-energy, and assuming  $x^0 > 0$  and  $y^0 > 0$ . Using eqs. (17,18) and transforming to spatial momentum space yields the Kadanoff-Baym equations for  $G_F(x^0, y^0, \mathbf{k})$  and  $G_{\rho}(x^0, y^0, \mathbf{k})$  for spatially homogeneous non-Gaussian initial states,

$$\begin{aligned}(\partial_{x^0}^2 + \mathbf{k}^2 + M^2(x^0)) G_F(x^0, y^0, \mathbf{k}) &= \int_0^{y^0} dz^0 \Pi_F(x^0, z^0, \mathbf{k}) G_{\rho}(z^0, y^0, \mathbf{k}) - \int_0^{x^0} dz^0 \Pi_{\rho}(x^0, z^0, \mathbf{k}) G_F(z^0, y^0, \mathbf{k}) \\ &\quad + \Pi_{\lambda\alpha, F}(x^0, \mathbf{k}) G_F(0, y^0, \mathbf{k}) + \frac{1}{4} \Pi_{\lambda\alpha, \rho}(x^0, \mathbf{k}) G_{\rho}(0, y^0, \mathbf{k}), \quad (20)\end{aligned}$$

and

$$(\partial_{x^0}^2 + \mathbf{k}^2 + M^2(x^0)) G_{\rho}(x^0, y^0, \mathbf{k}) = \int_{x_0}^{y^0} dz^0 \Pi_{\rho}(x^0, z^0, \mathbf{k}) G_{\rho}(z^0, y^0, \mathbf{k}),$$

where

$$\begin{aligned}\Pi_{\lambda\alpha, F}(x^0, \mathbf{k}) &= \Pi_{\lambda\alpha}^+(x^0, \mathbf{k}) + \Pi_{\lambda\alpha}^-(x^0, \mathbf{k}), \\ \Pi_{\lambda\alpha, \rho}(x^0, \mathbf{k}) &= 2i (\Pi_{\lambda\alpha}^+(x^0, \mathbf{k}) - \Pi_{\lambda\alpha}^-(x^0, \mathbf{k})).\end{aligned}$$

Thus, for a non-Gaussian initial state, the right-hand side of the Kadanoff-Baym equation for the statistical propagator is modified. In addition to the memory integrals there are now new contributions originating from the non-Gaussian initial correlations. Unlike the memory integrals, these new contributions do *not* have to vanish in the limit  $x^0, y^0 \rightarrow 0$ . This is due to the fact that the higher non-Gaussian correlations of the initial state can lead to a non-vanishing value of the connected four- and three-point correlation functions at the initial time.

### III. THERMAL INITIAL CORRELATIONS: PERTURBATION THEORY

In order to derive Kadanoff-Baym equations that are capable of describing thermal equilibrium, the thermal density matrix

$$\rho_{th} = \frac{1}{Z} \exp(-\beta H),$$

has to be represented by a Taylor expansion in terms of thermal correlation functions  $\alpha_n^{th}(x_1, \dots, x_n)$  as in eqs. (7, 8). These thermal correlation functions do then enter the Kadanoff-Baym equations in the form of non-local effective vertices, as described in the previous section.

The thermal correlations functions  $\alpha_n^{th}(x_1, \dots, x_n)$  can

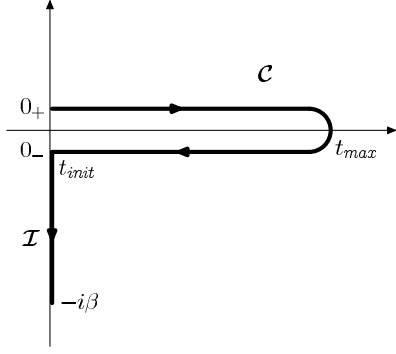


FIG. 5: The thermal time contour  $\mathcal{C}+\mathcal{I}$  is obtained by concatenating the closed real-time contour  $\mathcal{C}$  and the imaginary time contour  $\mathcal{I}$  running from  $t = 0$  to  $t = -i\beta$  [34–36].

be calculated order-by-order in the coupling constant within usual perturbation theory (see appendix A). However, in the Kadanoff-Baym context, it is necessary to use approximations of the thermal correlation functions that are compatible with the underlying truncation of the 2PI effective action. It is a major purpose of this paper to provide computational techniques for identifying suitable approximations of the thermal correlation functions  $\alpha_n^{th}(x_1, \dots, x_n)$ .

For simplicity, in this section, we first present the computational techniques within perturbation theory. In the following section, these techniques are then generalized to the nonperturbative 2PI formalism.

The main idea is to match the description of thermal equilibrium based on the closed real-time path  $\mathcal{C}$  in the presence of effective vertices  $\alpha_n^{th}(x_1, \dots, x_n)$  (“ $\mathcal{C}+\alpha$ ”) with the equivalent description based on the thermal time path (“ $\mathcal{C}+\mathcal{I}$ ”) [34–36] shown in figure 5.

The generating functional for these two descriptions is obtained by inserting the respective representations of the thermal density matrix,

$$\langle \varphi_+ | \rho_{th} | \varphi_- \rangle = \begin{cases} \int_{\varphi(0, \mathbf{x}) = \varphi_-(\mathbf{x})}^{\varphi(-i\beta, \mathbf{x}) = \varphi_+(\mathbf{x})} \mathcal{D}\varphi \exp\left(i \int_{\mathcal{I}} d^4x \mathcal{L}(x)\right) & \text{for “}\mathcal{C}+\mathcal{I}\text{”}, \\ \exp\left(i \sum_{n=0}^{\infty} \alpha_{12\dots n}^{th} \varphi_1 \varphi_2 \cdots \varphi_n\right) & \text{for “}\mathcal{C}+\alpha\text{”}, \end{cases} \quad (21)$$

into eq. (3). The argument of the exponential in the lower expression is a short-hand notation for eqs. (7, 8). In the following, we show how perturbative Feynman diagrams formulated within the  $\mathcal{C}+\mathcal{I}$  formalism can equivalently be represented within the  $\mathcal{C}+\alpha$  formalism.

### A. Thermal time contour $\mathcal{C}+\mathcal{I}$

The free thermal propagator defined on the thermal time contour  $\mathcal{C}+\mathcal{I}$  is

$$iG_{0,th}^{-1}(x, y) = (-\square_x - m^2) \delta_{\mathcal{C}+\mathcal{I}}(x - y),$$

for  $x^0, y^0 \in \mathcal{C}+\mathcal{I}$ . It may be decomposed into the free thermal statistical propagator  $G_{0,F}(x, y)$  and the free thermal spectral function  $G_{0,\rho}(x, y)$ ,

$$G_{0,th}(x, y) = G_{0,F}(x, y) - \frac{i}{2} \text{sign}_{\mathcal{C}+\mathcal{I}}(x^0 - y^0) G_{0,\rho}(x, y).$$

The explicit solution of the free equation of motion is

$$G_{0,F}(x^0, y^0, \mathbf{k}) = \frac{n_{BE}(\omega_k) + \frac{1}{2}}{\omega_k} \cos(\omega_k(x^0 - y^0)),$$

$$G_{0,\rho}(x^0, y^0, \mathbf{k}) = \frac{1}{\omega_k} \sin(\omega_k(x^0 - y^0)), \quad (22)$$

for  $x^0, y^0 \in \mathcal{C}+\mathcal{I}$ . Here,  $n_{BE}(\omega_k)$  is the Bose-Einstein distribution function,

$$n_{BE}(\omega_k) = \frac{1}{e^{\beta\omega_k} - 1}, \quad \omega_k = \sqrt{m^2 + \mathbf{k}^2}.$$

Each of the two time arguments of the propagator can either be real or imaginary, which yields four combinations  $G_{0,th}^{\mathcal{C}\mathcal{C}}, G_{0,th}^{\mathcal{C}\mathcal{I}}, G_{0,th}^{\mathcal{I}\mathcal{C}}, G_{0,th}^{\mathcal{I}\mathcal{I}}$ . These appear in perturbative Feynman diagrams which are constructed with the free propagator  $G_{0,th}$  and the classical vertices. In position space, each internal vertex of a Feynman diagram is integrated over the thermal time contour  $\mathcal{C}+\mathcal{I}$ . In order to disentangle the contributions from the real and the imaginary branch of the time contour, the following Feynman rules are defined,

$$G_{0,th}^{\mathcal{C}\mathcal{C}}(x, y) = \bullet \text{-----} \bullet, \quad G_{0,th}^{\mathcal{C}\mathcal{I}}(x, y) = \bullet \text{-----} \circ,$$

$$G_{0,th}^{\mathcal{I}\mathcal{I}}(x, y) = \circ \text{-----} \circ, \quad G_{0,th}^{\mathcal{I}\mathcal{C}}(x, y) = \circ \text{-----} \bullet,$$

$$-i\lambda \int_{\mathcal{C}} d^4x = \text{X}, \quad -i\lambda \int_{\mathcal{I}} d^4x = \text{X}, \quad -i\lambda \int_{\mathcal{C}+\mathcal{I}} d^4x = \text{X}.$$

The filled circles denote a real time, and the empty circles denote an imaginary time. As an example, the perturbative setting-sun diagram is considered with propagators attached to both external lines, and evaluated for real external times  $x^0, y^0 \in \mathcal{C}$ . Both internal vertices are integrated over the two branches  $\mathcal{C}$  and  $\mathcal{I}$ , respectively. Using the upper Feynman rules, the resulting four contributions can be depicted as

$$S_0(x, y) = \bullet \text{---} \circ \text{---} \bullet$$

$$= \frac{(-i\lambda)^2}{6} \int_{\mathcal{C}+\mathcal{I}} d^4u \int_{\mathcal{C}+\mathcal{I}} d^4v G_{0,th}(x, u) G_{0,th}^3(u, v) G_{0,th}(v, y)$$

$$= \bullet \text{---} \bullet \text{---} \bullet + \bullet \text{---} \circ \text{---} \bullet + \bullet \text{---} \circ \text{---} \bullet + \bullet \text{---} \bullet \text{---} \bullet$$

## B. Closed real-time contour with thermal initial correlations $\mathcal{C}+\alpha$

Within the  $\mathcal{C}+\alpha$  formalism, all internal vertices of Feynman diagrams are just integrated over the closed real-time path  $\mathcal{C}$ . However, the diagrams may contain non-local effective  $n$ -point vertices. These represent the  $n$ -point correlations  $\alpha_n^{th}(x_1, \dots, x_n)$  of the thermal initial state.

Let us consider a Feynman diagram within the  $\mathcal{C}+\mathcal{I}$  formalism, like for example the perturbative setting-sun diagram  $S_0(x, y)$ . We assume that all time arguments corresponding to the external lines are real. In the following, we will show how to obtain the same diagram within the  $\mathcal{C}+\alpha$  formalism. It turns out that a single diagram within the  $\mathcal{C}+\mathcal{I}$  formalism is represented by a set of diagrams within the  $\mathcal{C}+\alpha$  formalism. Some of these will contain non-local effective vertices. Since we are working in the framework of perturbation theory, we have to insert approximations to the exact effective vertices. For this purpose, we have to determine (i) the topologies of the required diagrams and (ii) the proper approximations for the effective vertices.

In order to do so, we first consider the free thermal propagator evaluated with one imaginary and one real time. Using eq. (22) together with elementary trigonometric addition theorems, it can be written as

$$G_{0,th}^{\mathcal{I}\mathcal{C}}(-i\tau, y^0, \mathbf{k}) = \frac{G_{0,th}^{\mathcal{I}\mathcal{I}}(-i\tau, 0, \mathbf{k})}{G_{0,th}(0, 0, \mathbf{k})} G_{0,F}^{\mathcal{C}\mathcal{C}}(0, y^0, \mathbf{k}) + i\partial_\tau G_{0,th}^{\mathcal{I}\mathcal{I}}(-i\tau, 0, \mathbf{k}) G_{0,\rho}^{\mathcal{C}\mathcal{C}}(0, y^0, \mathbf{k}).$$

Next, the unequal-time statistical propagator and the spectral function are rewritten as

$$G_{0,F}^{\mathcal{C}\mathcal{C}}(0, y^0, \mathbf{k}) = \int_{\mathcal{C}} dz^0 \delta_s(z^0) G_{0,th}^{\mathcal{C}\mathcal{C}}(z^0, y^0, \mathbf{k}),$$

$$G_{0,\rho}^{\mathcal{C}\mathcal{C}}(0, y^0, \mathbf{k}) = -2i \int_{\mathcal{C}} dz^0 \delta_a(z^0) G_{0,th}^{\mathcal{C}\mathcal{C}}(z^0, y^0, \mathbf{k}),$$

where

$$\delta_s(z^0) = \frac{1}{2} (\delta_{\mathcal{C}}(z^0 - 0_+) + \delta_{\mathcal{C}}(z^0 - 0_-)),$$

$$\delta_a(z^0) = \frac{1}{2} (\delta_{\mathcal{C}}(z^0 - 0_+) - \delta_{\mathcal{C}}(z^0 - 0_-)).$$

Combining the upper equations, a helpful expression for the free propagator evaluated with one imaginary and one real time is obtained,

$$G_{0,th}^{\mathcal{I}\mathcal{C}}(-i\tau, y^0, \mathbf{k}) = \int_{\mathcal{C}} dt \Delta_0(-i\tau, t, \mathbf{k}) G_{0,th}^{\mathcal{C}\mathcal{C}}(t, y^0, \mathbf{k}),$$

$$\circ \text{-----} \bullet = \circ \text{.....} | \text{-----} \bullet. \quad (23)$$

Here, the *free connection*  $\Delta_0(-i\tau, z^0, \mathbf{k})$  is given by

$$\Delta_0(-i\tau, z^0, \mathbf{k}) = \Delta_0^s(-i\tau, \mathbf{k}) \delta_s(z^0) + \Delta_0^a(-i\tau, \mathbf{k}) \delta_a(z^0)$$

$$= \text{.....} | \text{---}, \quad (24)$$

where

$$\Delta_0^s(-i\tau, \mathbf{k}) = \frac{G_{0,th}^{\mathcal{I}\mathcal{I}}(-i\tau, 0, \mathbf{k})}{G_{0,th}(0, 0, \mathbf{k})},$$

$$\Delta_0^a(-i\tau, \mathbf{k}) = 2\partial_\tau G_{0,th}^{\mathcal{I}\mathcal{I}}(-i\tau, 0, \mathbf{k}). \quad (25)$$

Analogously, the free propagator evaluated with one real and one imaginary time can be written as

$$G_{0,th}^{\mathcal{C}\mathcal{I}}(y^0, -i\tau, \mathbf{k}) = \int_{\mathcal{C}} dt G_{0,th}^{\mathcal{C}\mathcal{C}}(x^0, t, \mathbf{k}) \Delta_0^T(t, -i\tau, \mathbf{k}),$$

$$\bullet \text{-----} \circ = \bullet \text{---} | \text{.....} \circ,$$

where  $\Delta_0^T(z^0, -i\tau, \mathbf{k}) = \Delta_0(-i\tau, z^0, \mathbf{k}) = \text{---} | \text{.....}$ . The connections  $\Delta_0$  and  $\Delta_0^T$  are attached to an imaginary and a real vertex on the left and right sides, respectively. Their Fourier transform into position space is

$$\Delta_0(v, z) = \int \frac{d^3\mathbf{k}}{(2\pi)^3} e^{i\mathbf{k}(v-z)} \Delta_0(v^0, z^0, \mathbf{k}), \quad (26)$$

for  $v^0 \in \mathcal{I}$  and  $z^0 \in \mathcal{C}$ , as well as  $\Delta_0^T(z, v) = \Delta_0(v, z)$ .

In general, for any thermal diagram on  $\mathcal{C}+\mathcal{I}$  with  $\mathcal{V}$  internal vertices, there are  $2^{\mathcal{V}}$  possibilities to combine the integration over  $\mathcal{C}$  or  $\mathcal{I}$  at each vertex. For each of these  $2^{\mathcal{V}}$  contributions, all lines connecting a real and an imaginary vertex are replaced using relation (23). Thereby the parts containing  $\mathcal{I}$ -integrations are encapsulated into non-local effective vertices. Thus, any thermal diagram on  $\mathcal{C}+\mathcal{I}$  can equivalently be represented by  $2^{\mathcal{V}}$  diagrams on  $\mathcal{C}$ , which contain classical vertices as well as non-local effective vertices.

For example, the setting-sun diagram with one real and one imaginary vertex can be rewritten as

$$\bullet \text{---} \circ \text{---} \bullet = \bullet \text{---} \circ \text{---} | \text{---} \bullet \equiv \bullet \text{---} \boxed{\circ} \text{---} \bullet \equiv \bullet \text{---} \circ \text{---} \text{th}_{OL} \bullet \quad (27)$$

According to the symbolic notation employed here, the subdiagram containing the imaginary vertex, marked by the box, can be encapsulated into an effective non-local 4-point vertex. Its structure is determined by the connections  $\Delta_0$  and  $\Delta_0^T$ . This can be seen by rewriting the above diagrams in terms of the corresponding formal expressions (only the first and last one are given here),

$$\frac{(-i\lambda)^2}{6} \int_{\mathcal{C}} d^4u \int_{\mathcal{I}} d^4v G_{0,th}(x, u) G_{0,th}^3(u, v) G_{0,th}(v, y)$$

$$\equiv \frac{-i\lambda}{6} \int_{\mathcal{C}} d^4u \int_{\mathcal{C}} d^4z_{1234} G_{0,th}(x, u) G_{0,th}(u, z_1) G_{0,th}(u, z_2)$$

$$\times G_{0,th}(u, z_3) \left[ \alpha_{4,0L}^{th}(z_1, z_2, z_3, z_4) \right] G_{0,th}(z_4, y).$$

In the last line, the thermal effective 4-point vertex has





The derivation of this equation is also shown in appendix B. Similar to the perturbative case, the formalism established above can be used to relate any Feynman diagram formulated on the thermal time path (“ $\mathcal{C}+\mathcal{I}$ ”) with a set of Feynman diagrams formulated on the closed real-time path  $\mathcal{C}$  containing non-local effective vertices representing the thermal initial correlations (“ $\mathcal{C}+\alpha$ ”). This is accomplished by three steps:

1. First, the contour integrations over the thermal time path  $\mathcal{C}+\mathcal{I}$  associated with internal vertices are split into two integrations over  $\mathcal{C}$  and  $\mathcal{I}$ . A diagram with  $\mathcal{V}$  vertices is thus decomposed into  $2^{\mathcal{V}}$  contributions.
2. Second, all internal propagator lines connecting a real and an imaginary time are replaced using eq. (30). Additionally, the internal propagator lines connecting two imaginary times are replaced according to eq. (B13). The parts containing imaginary times are encapsulated, which can be visualized by joining the complete “connections” to boxes surrounding the imaginary vertices.
3. Third, the iterative solution of eq. (31) for the complete connection is inserted. Each resulting contribution can be identified as a diagram formulated on the closed real-time path  $\mathcal{C}$  containing non-local effective vertices  $\alpha_n$ . The latter are constructed explicitly, as appropriate for the underlying 2PI approximation.

The first two steps are analogous to the perturbative case, with complete propagators and connections instead of free ones. The third step is special for the nonperturbative case. It results in contributions which contain non-local effective vertices  $\alpha_n$  of arbitrarily high order  $n$ . These take into account the infinite sequence of thermal initial  $n$ -point correlations, which are present due to the underlying nonperturbative approximation.

For example, for the nonperturbative setting sun diagram, step one and two can be written as

$$\begin{aligned}
 S(x, y) = & \text{---} \circ \text{---} + \text{---} \boxed{\circ} \text{---} + \text{---} \boxed{\circ} \text{---} \\
 & + \text{---} \boxed{\circ} \boxed{\circ} \text{---} + \text{---} \boxed{\circ} \boxed{\circ} \text{---} + \text{---} \boxed{\circ} \boxed{\circ} \text{---} \\
 & + \text{---} \boxed{\circ} \boxed{\circ} \text{---} .
 \end{aligned}$$

For the second diagram, the third step can be written as

$$\begin{aligned}
 \text{---} \boxed{\circ} \text{---} = & \text{---} \boxed{\circ} \text{---} + \text{---} \boxed{\circ} \text{---} \\
 & + \text{---} \boxed{\circ} \text{---} + \text{---} \boxed{\circ} \text{---} + \text{---} \boxed{\circ} \text{---} \\
 & + \text{---} \boxed{\circ} \text{---} + \text{---} \boxed{\circ} \text{---} + \text{---} \boxed{\circ} \text{---} + \dots
 \end{aligned}$$

The first diagram on the right-hand side is obtained by inserting the zeroth iteration for the four complete connections. The other diagrams are obtained by inserting the first iteration. Note that all diagrams shown above are generated with correct symmetry factors.

Each of the boxes with thin lines represents a non-local effective vertex, encoding the correlations of the initial state. A thin box which is attached to  $n$  propagator lines represents a contribution to the thermal initial  $n$ -point correlation function  $\alpha_n^{th}(x_1, \dots, x_n)$ . For example, the leading contributions to the thermal initial 4- and 6-point correlations are given by

$$\begin{aligned}
 \alpha_{4,0L}^{th,2PI}(z_1, \dots, z_4) \\
 = -i\lambda \int_{\mathcal{I}} d^4v \Delta^{(0)}(v, z_1) \Delta^{(0)}(v, z_2) \Delta^{(0)}(v, z_3) \Delta^{(0)}(v, z_4)
 \end{aligned}$$

$$\boxed{\text{---}}_{0L}^{th,2PI} = \text{---} \times \text{---} \times \text{---} \times \text{---} \equiv \text{---} \boxed{\times} \text{---}, \quad (34)$$

and

$$\begin{aligned}
 \alpha_{6,0L}^{th,2PI}(z_1, \dots, z_6) \\
 = (-i\lambda)^2 \int_{\mathcal{I}} d^4v \int_{\mathcal{I}} d^4w \Delta^{(0)}(v, z_1) \Delta^{(0)}(v, z_2) \Delta^{(0)}(v, z_3) \\
 \times D(v, w) \Delta^{(0)}(w, z_4) \Delta^{(0)}(w, z_5) \Delta^{(0)}(w, z_6),
 \end{aligned}$$

$$\boxed{\text{---}}_{0L}^{th,2PI} = \text{---} \boxed{\times} \text{---} \boxed{\times} \text{---} \equiv \text{---} \boxed{\times} \text{---}. \quad (35)$$

Note that these contributions are nonperturbative approximations of the exact thermal initial correlations, since they involve the complete thermal propagator.

## V. KADANOFF-BAYM EQUATIONS WITH THERMAL INITIAL CORRELATIONS

In this section, Kadanoff-Baym equations that can describe thermal equilibrium on the closed real-time path  $\mathcal{C}$  with finite initial time  $t_{init} = 0$  are derived. Therefore, it is required to take into account non-Gaussian correlations of the initial (thermal) state of the system. These thermal initial correlations have to be determined in accordance with the nonperturbative 2PI formalism underlying the Kadanoff-Baym equations. Therefore, the techniques developed in the previous section are combined with the Kadanoff-Baym equations for non-Gaussian initial states derived in section II.

The Kadanoff-Baym equation for a thermal initial state is a special case of the Kadanoff-Baym equation for a non-Gaussian initial state (see eq. (19)), which has

the form

$$\begin{aligned}
& (\partial_{x^0}^2 + \mathbf{k}^2 + M_{th}^2) G_{th}(x^0, y^0, \mathbf{k}) = -i\delta_{\mathcal{C}}(x^0 - y^0) \\
& - i \int_{\mathcal{C}} dz^0 \left[ \Pi_{th,nl}^G(x^0, z^0, \mathbf{k}) + \Pi_{th,nl}^{nG}(x^0, z^0, \mathbf{k}) \right. \\
& \left. + i\Pi_{th,\lambda\alpha}(x^0, z^0, \mathbf{k}) \right] G_{th}(z^0, y^0, \mathbf{k}). \quad (36)
\end{aligned}$$

Here  $\Pi_{th,nl}^G(x^0, z^0, \mathbf{k})$  and  $\Pi_{th,nl}^{nG}(x^0, z^0, \mathbf{k})$  denote the Gaussian- and non-Gaussian parts of the non-local self-energy, respectively. Furthermore,

$$\begin{aligned}
& \Pi_{th,\lambda\alpha}(x^0, z^0, \mathbf{k}) \\
& = \Pi_{th,\lambda\alpha,F}(x^0, \mathbf{k})\delta_s(z^0) - \frac{i}{2}\Pi_{th,\lambda\alpha,\rho}(x^0, \mathbf{k})\delta_a(z^0)
\end{aligned}$$

denotes the contribution from the non-Gaussian initial correlations which is supported at the initial time surface  $z^0 = 0$  (see section II).

The equation of motion of the complete thermal propagator based on the thermal time contour (“ $\mathcal{C}+\mathcal{I}$ ”) evaluated for  $x^0, y^0 \in \mathcal{C}$  is

$$\begin{aligned}
& (\partial_{x^0}^2 + \mathbf{k}^2 + M_{th}^2) G_{th}(x^0, y^0, \mathbf{k}) = -i\delta_{\mathcal{C}+\mathcal{I}}(x^0 - y^0) \\
& - i \int_{\mathcal{C}+\mathcal{I}} dz^0 \Pi_{th}^{nl}(x^0, z^0, \mathbf{k}) G_{th}(z^0, y^0, \mathbf{k}). \quad (37)
\end{aligned}$$

The integral over the imaginary-time contour  $\mathcal{I}$  can be rewritten using the complete connection (31),

$$\begin{aligned}
& \int_{\mathcal{I}} dz^0 \Pi_{th}^{nl}(x^0, z^0, \mathbf{k}) G_{th}(z^0, y^0, \mathbf{k}) \\
& = \int_{\mathcal{I}} dv^0 \Pi_{th}^{nl}(x^0, v^0, \mathbf{k}) \int_{\mathcal{C}} dz^0 \Delta(v^0, z^0, \mathbf{k}) G_{th}(z^0, y^0, \mathbf{k}) \\
& = \int_{\mathcal{C}} dz^0 \int_{\mathcal{I}} dv^0 \Pi_{th}^{nl}(x^0, v^0, \mathbf{k}) \left( \Delta^{(0)}(v^0, z^0, \mathbf{k}) \right. \\
& \left. + \int_{\mathcal{I}} dw^0 D(v^0, w^0, \mathbf{k}) \Pi_{th}^{nl}(w^0, z^0, \mathbf{k}) \right) G_{th}(z^0, y^0, \mathbf{k}).
\end{aligned}$$

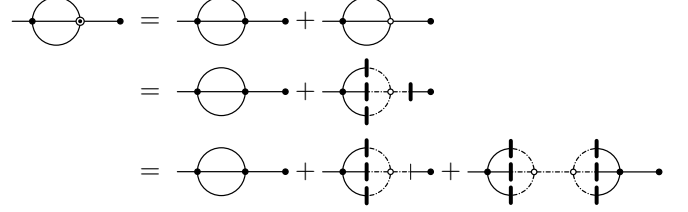
Inserting this into the equation of motion (37), it takes precisely the form of the Kadanoff-Baym equation for a non-Gaussian initial state. By comparison, the non-Gaussian contributions to the self-energy for the thermal initial state can be inferred,

$$\Pi_{th,nl}^G(x^0, z^0, \mathbf{k}) = \Pi_{th}^{nl}(x^0, z^0, \mathbf{k}) \Big|_{x^0, z^0 \in \mathcal{C}}, \quad (38)$$

$$\begin{aligned}
\Pi_{th,nl}^{nG}(x^0, z^0, \mathbf{k}) & = \int_{\mathcal{I}} dv^0 \int_{\mathcal{I}} dw^0 \Pi_{th}^{nl}(x^0, v^0, \mathbf{k}) \\
& \times D(v^0, w^0, \mathbf{k}) \Pi_{th}^{nl}(w^0, z^0, \mathbf{k}) \Big|_{x^0, z^0 \in \mathcal{C}},
\end{aligned}$$

$$\begin{aligned}
i\Pi_{th,\lambda\alpha}(x^0, z^0, \mathbf{k}) & = \int_{\mathcal{I}} dv^0 \Pi_{th}^{nl}(x^0, v^0, \mathbf{k}) \\
& \times \Delta^{(0)}(v^0, z^0, \mathbf{k}) \Big|_{x^0, z^0 \in \mathcal{C}}.
\end{aligned}$$

For the setting-sun approximation, the steps listed above leading from the formulation of the Schwinger-Dyson equation on the thermal time path (“ $\mathcal{C}+\mathcal{I}$ ”) to the formulation on the closed real-time path with thermal initial correlations (“ $\mathcal{C}+\alpha$ ”) are



Thus, the Gaussian and non-Gaussian contributions to the self-energy in setting-sun approximation for a thermal initial state are given by

$$\begin{aligned}
\Pi_{th,nl}^G(x^0, z^0, \mathbf{k}) & = \text{circle with dot on left and dot on right}, \\
\Pi_{th,nl}^{nG}(x^0, z^0, \mathbf{k}) & = \text{circle with dot on left and dot on right, plus circle with dot on left and dot on right, plus circle with dot on left and dot on right}, \\
i\Pi_{th,\lambda\alpha}(x^0, z^0, \mathbf{k}) & = \text{circle with dot on left and dot on right, plus circle with dot on left and dot on right}. \quad (39)
\end{aligned}$$

In order to explicitly obtain the thermal initial correlations which are appropriate for a specific 2PI approximation, the iterative expansion (32) of the complete connection has to be inserted. This yields a series expansion of the non-Gaussian self-energies,

$$\Pi_{th,\lambda\alpha} = \sum_{k=0}^{\infty} \Pi_{th,\lambda\alpha}^{(k)}, \quad \Pi_{th,nl}^{nG} = \sum_{k=0}^{\infty} \Pi_{th,nl}^{(k),nG},$$

where

$$\begin{aligned}
\Pi_{th,\lambda\alpha}^{(0)} & = \Pi_{th,\lambda\alpha} \Big|_{\Delta^{(0)}}, \\
\Pi_{th,\lambda\alpha}^{(k)} & = \Pi_{th,\lambda\alpha} \Big|_{\Delta^{(k)}} - \Pi_{th,\lambda\alpha}^{(k-1)},
\end{aligned}$$

and analogously for  $\Pi_{th,nl}^{nG}$ .

For example, in setting-sun approximation, the thermal initial correlations obtained from inserting the zeroth, first and second iteration of the complete connec-

tion are

$$\begin{aligned}
i\Pi_{th,\lambda\alpha}^{(0)} &= \text{diagram} = \text{diagram}^{th, 2PI}_{0L}, \quad (40) \\
i\Pi_{th,\lambda\alpha}^{(1)} &= \text{diagram} + \text{diagram} + \text{diagram}, \\
i\Pi_{th,\lambda\alpha}^{(2)} &= \text{diagram} + \dots + \text{diagram}.
\end{aligned}$$

The zeroth contribution contains the thermal non-local effective 4-point vertex (34). The first iteration yields three diagrams with thermal effective 6-, 8-, and 10-point vertices, and the second iteration yields six contributions with thermal effective 8-, 10-, 12- (two diagrams), 14-, and 16-point vertices. The smallest and largest are shown in the last line of eq. (40). The expansion of  $\Pi_{th,nl}^{nG}$  contains thermal non-local effective vertices of order six and higher,

$$\begin{aligned}
\Pi_{th,nl}^{(0),nG} &= \text{diagram} = \text{diagram}^{th, 2PI}_{0L}, \\
\Pi_{th,nl}^{(1),nG} &= \text{diagram} + \text{diagram} \\
&+ \dots + \text{diagram}.
\end{aligned}$$

The zeroth contribution contains the thermal non-local effective 6-point vertex (35). The first contribution contains 15 diagrams with thermal effective vertices of order 8 to 18. The order of the thermal initial correlations appearing up to the fifth contribution in setting-sun approximation are shown in table I.

Thus, vacuum or thermal initial states entail an infinite hierarchy of initial  $n$ -point correlation functions. In setting-sun approximation, the non-Gaussian initial correlation of lowest order is the 4-point correlation given in the first line of eq. (40). Its contribution to the Kadanoff-Baym equations is

$$\begin{aligned}
i\Pi_{th,\lambda\alpha}^{(0)}(x, z) &= \frac{-i\lambda}{6} \int_{\mathcal{C}} d^4x_{123} G_{th}(x, x_1) G_{th}(x, x_2) \\
&\times G_{th}(x, x_3) i\alpha_{4,0L}^{th, 2PI}(x_1, x_2, x_3, z).
\end{aligned}$$

In the limit  $x^0, y^0 \rightarrow 0$ , only the thermal initial 4-point correlation contributes to the right-hand side of the Ka-

$$\Pi_{th,\lambda\alpha}(x^0, z^0, \mathbf{k})$$

	4	6	8	10	12	14	16	...	22	...	28	...	34	...
0	×													
1		×	×	×										
2			×	×	×	×	×							
3				×	×	×	×	...	×					
4					×	×	×	...	×	...	×	...	×	
5						×	×	...	×	...	×	...	×	...
...														

$$\Pi_{th,nl}^{nG}(x^0, z^0, \mathbf{k})$$

	4	6	8	10	12	14	16	18	...	30	...	42	...	54	...	66	...
0	×																
1		×	×	×	×	×	×										
2			×	×	×	×	×	...	×								
3				×	×	×	×	...	×	...	×	...	×				
4					×	×	×	...	×	...	×	...	×	...	×		
5						×	×	...	×	...	×	...	×	...	×	...	×
...																	

TABLE I: *Thermal initial correlations in 2PI setting-sun approximation. The column number is the order  $n = 4, 6, \dots$  of the thermal initial  $n$ -point correlation. The row number  $k = 0, 1, \dots$  shows which initial correlations contribute to  $\Pi_{th,\lambda\alpha}^{(k)}$  (upper table) and  $\Pi_{th,nl}^{(k),nG}$  (lower table), respectively. Due to the  $Z_2$ -symmetry, only even correlations are non-zero.*

danoff-Baym equations (36),

$$\begin{aligned}
&\int_{\mathcal{C}} dz^0 [\Pi_{th,nl}^{nG} + \Pi_{th,nl}^{nG} + i\Pi_{th,\lambda\alpha}^{(0)}](x^0, z^0, \mathbf{k}) G_{th}(z^0, y^0, \mathbf{k}) \\
&\rightarrow \int_{\mathcal{C}} dz^0 i\Pi_{th,\lambda\alpha}^{(0)}(x^0, z^0, \mathbf{k}) G_{th}(z^0, y^0, \mathbf{k}), \quad (41)
\end{aligned}$$

for  $x^0, y^0 \rightarrow 0$ . The reason is that all other contributions contain at least one internal classical vertex. However, these vertices are accompanied by memory integrals. Due to the structure of the closed real time-path, memory integrals vanish when all external time arguments approach the initial time.

Altogether, Kadanoff-Baym equations that describe thermal equilibrium have been derived on the closed real-time path with finite initial time. This requires to take into account non-Gaussian  $n$ -point correlations of the initial state, which enter explicitly on the right-hand side of the Kadanoff-Baym equations. The values of these initial correlation functions for a thermal state can be determined iteratively in accordance with the underlying 2PI approximation.

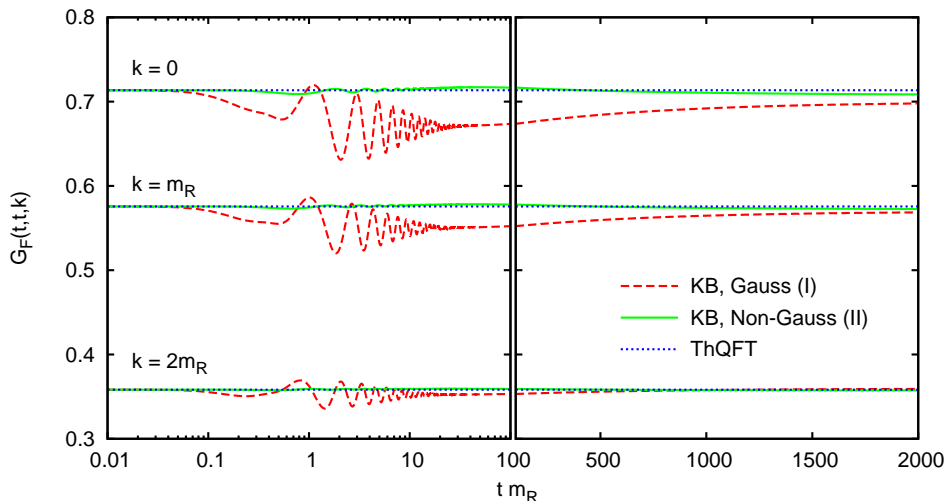


FIG. 6: Time evolution of the equal-time propagator  $G_F(t, t, \mathbf{k})$  obtained from Kadanoff-Baym equations with thermal initial 2-point correlation function (initial state (A), red dashed lines) as well as thermal initial 2- and 4-point correlation functions (initial state (B), green solid lines), for three momentum modes, respectively. The dotted horizontal lines show the renormalized thermal propagator  $G_{th}(0, 0, \mathbf{k})$  which serves as initial condition at  $t = 0$ .

## VI. NUMERICAL RESULTS

In this section, we support the findings of the previous section by numerical solutions of Kadanoff-Baym equations. Of course, one cannot implement the complete infinite hierarchy of initial  $n$ -point correlation functions, which would be required for an exact description of thermal equilibrium in the framework of Kadanoff-Baym equations. However, thermal equilibrium can be approached closer and closer as one includes more and more thermal initial correlations. Therefore, we consider initial states which are obtained by keeping thermal initial  $n$ -point correlation functions for  $n \leq n_{max}$  and setting all higher initial correlations to zero,

$$\alpha_n(x_1, \dots, x_n) = \begin{cases} \alpha_n^{th}(x_1, \dots, x_n) & \text{for } n \leq n_{max}, \\ 0 & \text{for } n > n_{max}. \end{cases}$$

More precisely, we compare the time evolution obtained for two  $Z_2$ -symmetric initial states (A) and (B) with  $n_{max} = 2$  and  $n_{max} = 4$ , respectively. Both initial states have in common that the statistical propagator is initialized with the thermal propagator and that all initial correlations  $\alpha_n(x_1, \dots, x_n)$  with  $n > 4$  vanish:

$$\begin{aligned} G_F(x^0, y^0, \mathbf{k})|_{x^0=y^0=0} &= G_{th}(-i\tau, 0, \mathbf{k})|_{\tau \rightarrow 0}, \\ \partial_{x^0} G_F(x^0, y^0, \mathbf{k})|_{x^0=y^0=0} &= 0, \\ \partial_{x^0} \partial_{y^0} G_F(x^0, y^0, \mathbf{k})|_{x^0=y^0=0} &= \partial_\tau^2 G_{th}(-i\tau, 0, \mathbf{k})|_{\tau \rightarrow 0}, \\ \alpha_n(x_1, \dots, x_n) &= 0, \quad \text{for } n > 4 \end{aligned}$$

where  $G_{th}(-i\tau, 0, \mathbf{k})$  is the complete thermal propagator at temperature  $T = T_{init}$ . The only difference is in the

initial 4-point correlation:

$$\alpha_4(x_1, \dots, x_4) = \begin{cases} 0 & \text{for (A)}, \\ \alpha_4^{th}(x_1, \dots, x_4) & \text{for (B)}, \end{cases}$$

where  $\alpha_4^{th}(x_1, \dots, x_4)$  is chosen as shown in eq. (40). Accordingly, (A) is a Gaussian initial state and (B) is a minimal non-Gaussian initial state, and both states “are as thermal as possible” for the respective classes of initial states.

In both cases, we employ the 2PI three-loop approximation as discussed in Ref. [9] and section II.

The numerical solutions were obtained on a lattice with  $32^3 \times 2000^2$  lattice sites and lattice spacings of  $a_s m_R = 0.5$  and  $a_t m_R = 0.025$ . We use  $\lambda_R/4! = 0.75$  for the renormalized coupling constant. The bare mass  $m_B$  and coupling  $\lambda_B$ , as well as the thermal propagator  $G_{th}(-i\tau, 0, \mathbf{k})$  are determined by a separate numerics program as described in Refs. [28, 29].

### A. Time-evolution of the equal-time propagator

Both initial states (A) and (B) are nonequilibrium initial states, since the thermal initial correlations higher than  $n_{max}$  are discarded. However, among all possible Gaussian initial states, the state (A) has the minimal offset from thermal equilibrium. Similarly, the state (B) has the minimal offset from equilibrium among all possible initial states that are parameterized by initial 2- and 4-point correlation functions. In the following, we will compare this *minimal offset* for both initial states (A) and (B). In exact thermal equilibrium, the equal-time

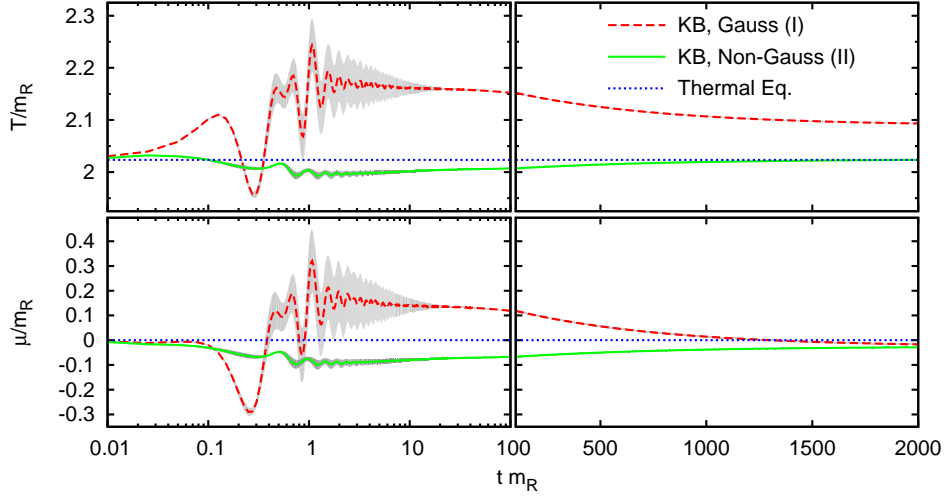


FIG. 7: Time evolution of the effective temperature and chemical potential obtained from Kadanoff-Baym equations with thermal initial 2-point correlation function (initial state (A), red dashed lines) as well as thermal initial 2- and 4-point correlation functions (initial state (B), green solid lines). The shaded areas illustrate qualitatively the deviation of the effective particle number density  $n(t, \mathbf{k})$  from the Bose-Einstein distribution function. They are obtained from the asymptotic standard error of the fit (via least-square method) magnified by a factor 10, for better visibility. Nevertheless, the errors become invisibly small at times  $tm_R \gg 10$ .

propagator  $G_F(t, t, \mathbf{k})$  is constant. Therefore, the time-dependence of the equal-time propagator is a measure for the deviation from thermal equilibrium.

Figure 6 shows the time-evolution of the equal-time propagator obtained from the numerical solution of the two sets of Kadanoff-Baym equations. We find that the deviation from thermal equilibrium is considerable for the Kadanoff-Baym equations with Gaussian initial state (A). In contrast to this, for the Kadanoff-Baym equations with the non-Gaussian initial state (B) the equal-time propagator remains very close to the thermal propagator at all times. We have checked that this qualitative behaviour stays the same when varying the coupling strength or the lattice spacings. This shows that the thermal initial 4-point correlation already yields a reasonable approximation of the complete thermal initial state.

This observation can be understood by analyzing the role of the thermal initial correlations (39) in the Kadanoff-Baym equations (20). In fact, there are two distinct reasons why the contribution of the thermal initial  $n$ -point correlations are suppressed for  $n > 4$ .

The first reason is that the effective loss of memory is stronger the larger  $n$ . This can be seen as follows: The thermal initial  $n$ -point correlations enter the Kadanoff-Baym equations as effective  $n$ -point vertices. These are connected with classical vertices by  $n$  lines. Each of these lines yields a propagator  $G(t, 0, \mathbf{k})$  for which one of the time arguments is evaluated at the initial time (see eq. (9)). However, such unequal-time propagators are damped exponentially with respect to the time  $t$  [5]. Therefore the contribution of the initial  $n$ -point correlations is also damped exponentially for  $t \rightarrow \infty$ , and the

damping is the stronger the larger  $n$ .

The second reason is that the contributions to the Kadanoff-Baym equations (20) which arise from thermal initial  $n$ -point correlations with  $n > 4$ , vanish in the limit  $t \rightarrow 0$  as has been shown in section V.

Thus, the influence of thermal initial  $n$ -point correlations with  $n > 4$  on the solutions of Kadanoff-Baym equations is suppressed compared to the initial 4-point correlation for early times ( $t \rightarrow 0$ ) as well as for late times ( $t \rightarrow \infty$ ).

## B. Offset between initial and final temperature

Figure 7 shows the time-evolution of the effective temperature  $T(t)$  and chemical potential  $\mu(t)$ . They are obtained by fitting a Bose-Einstein distribution function to the effective particle number density  $n(t, \mathbf{k})$  for all times  $t$ . The effective particle number density can directly be extracted from solutions of Kadanoff-Baym equations [9]. At the initial time, we have  $T(0) = T_{init}$  and  $\mu(0) = 0$ . For  $t \rightarrow \infty$ , the solutions approach thermal equilibrium<sup>4</sup>, i.e.  $T(t) \rightarrow T_{final}$  and  $\mu(t) \rightarrow 0$  within the numerical accuracy. The time-evolution can be divided into the three phases of (i) correlation build-up for  $tm_R \lesssim 1$ , (ii) kinetic equilibration for  $1 \lesssim tm_R \lesssim 10$  and (iii) chemical equilibration for  $tm_R \gtrsim 10$ . The numerical solutions clearly

---

<sup>4</sup> For  $\lambda\Phi^4$ -theory, the chemical potential in equilibrium is zero, since particle number is not conserved.

exhibit a separation between the time-scales of kinetic and chemical equilibration [9, 18].

We see in figure 7 that the deviation from thermal equilibrium is much smaller for the non-Gaussian initial state (B) as compared to the Gaussian initial state (A). This result supports the observation from the previous subsection.

In addition, figure 7 reveals a qualitative difference between both sets of equations. For the Gaussian initial condition (A), an offset between the initial temperature  $T_{init}$  and the final temperature  $T_{final}$  occurs. However, for the non-Gaussian initial condition (B), the initial and final value of the temperature agree within the numerical accuracy.

This behaviour can be explained by looking at the total energy of the system. It can be split into kinetic and correlation energy,

$$E_{total} = E_{kin}(t) + E_{corr}(t) , \quad (42)$$

where

$$E_{kin}(t) = \frac{1}{2} \int \frac{d^3 k}{(2\pi)^3} \left[ \partial_{x^0} \partial_{y^0} + \mathbf{k}^2 + m^2 \right. \\ \left. + \frac{\lambda}{4} \int \frac{d^3 q}{(2\pi)^3} G_F(t, t, \mathbf{q}) \right] G_F(x^0, y^0, \mathbf{k})|_{x^0=y^0=t} ,$$

$$E_{corr}(t) = -\frac{1}{4} \int \frac{d^3 k}{(2\pi)^3} \left[ \left( \Pi_{\lambda\alpha, F}(t, \mathbf{k}) G_F(0, t, \mathbf{k}) \right. \right. \\ \left. \left. + \frac{1}{4} \Pi_{\lambda\alpha, \rho}(t, \mathbf{k}) G_\rho(0, t, \mathbf{k}) \right) \right. \\ \left. - \int_0^t dz^0 \left( \Pi_F(t, z^0, \mathbf{k}) G_\rho(z^0, t, \mathbf{k}) \right) \right. \\ \left. - \Pi_\rho(t, z^0, \mathbf{k}) G_F(z^0, t, \mathbf{k}) \right] .$$

The total energy is conserved by the numerical solutions up to numerical errors ( $< 1\%$ ). Using the thermal initial state, we can also derive an expression for the total energy in thermal equilibrium at temperature  $T$ ,

$$E^{eq}(T) = E_{kin}^{eq}(T) + E_{corr}^{eq}(T) ,$$

where  $E_{kin}^{eq}(T) = E_{kin}(t=0)|_{G=G_{th}}$  and

$$E_{corr}^{eq}(T) = -\frac{1}{4} \int \frac{d^3 k}{(2\pi)^3} \Pi_{th, \lambda\alpha, F}(t, \mathbf{k}) G_{th}(0, t, \mathbf{k})|_{t=0} .$$

For all possible initial states, the final temperature can then be determined by the requirement

$$E_{total} = E^{eq}(T_{final}) .$$

Both initial states considered here feature thermal  $n$ -point correlations at temperature  $T_{init}$  for  $n \leq n_{max}$ . Therefore, we have

$$E_{total} = E^{eq}(T_{init}) - \Delta E_{(n>n_{max})}(T_{init}) ,$$

where  $\Delta E_{(n>n_{max})}(T)$  denotes the contribution to the thermal energy that comes from  $n$ -point correlations with  $n > n_{max}$ . For initial state (A), we find

$$\Delta E_{(n>2)}(T) = E_{corr}^{eq}(T) .$$

Since the thermal correlation energy has a non-zero value, we find that

$$T_{final} \neq T_{init} \quad \text{for initial state (A).}$$

This is in accordance with the results of Ref. [22] for the non-relativistic case. In general, one would expect that this is also true for initial state (B). However, using eq. (41), we obtain

$$E_{corr}^{eq}(T) = \frac{\lambda}{4!} \int_{\mathcal{C}} d^4 x_{1234} G_{th}(x, x_1) G_{th}(x, x_2) \\ \times G_{th}(x, x_3) i\alpha_4^{th}(x_1, x_2, x_3, x_4) G_{th}(x_4, x)|_{x=0} .$$

Thus, only the initial 4-point correlation contributes to the thermal correlation energy. Therefore we have  $\Delta E_{(n>4)}(T) = 0$ , which means that the initial and final temperatures have to agree,

$$T_{final} = T_{init} \quad \text{for initial state (B).}$$

This property is quite remarkable. It means that the total energies for the initial state (B) and for the complete thermal initial state are identical. Thus, the thermal initial  $n$ -point correlations  $\alpha_n^{th}$  with  $n > 4$  do not contribute to the total energy of the initial state. Instead, the thermal initial 4-point correlation  $\alpha_4^{th}$  already captures the complete thermal correlation energy at the initial time in setting-sun approximation.

Moreover, this result can be generalized to arbitrary 2PI approximations. In general, the correlation energy at the initial time is given by

$$E_{corr}(t=0) = -\frac{1}{4} \int \frac{d^3 k}{(2\pi)^3} \Pi_{\lambda\alpha, F}(t, \mathbf{k}) G_F(0, t, \mathbf{k})|_{t=0} .$$

The most general structure of the non-Gaussian self-energy  $\Pi_{\lambda\alpha}(x, y)$  is shown in figure 8. The Kernels  $A_4^{nG}$  and  $A_3^{nG}$  may in general contain classical as well as non-local effective vertices. In setting-sun approximation (13), they are given by  $A_4^{nG} = \alpha_4$  and  $A_3^{nG} = 0$ . In the limit  $t \equiv x^0 \rightarrow 0$ , all contributions containing classical vertices vanish due to the memory integrals accompanying these vertices. Thus, at the initial time, only those parts of  $A_4^{nG}$  and  $A_3^{nG}$  do contribute to the correlation energy that can be rewritten in the form of an initial 4- and 3-point vertex, respectively.

This property is characteristic for the  $\Phi^4$ -interaction. If the Lagrangian would contain a (non-renormalizable)  $\Phi^6$ -interaction, then also initial 5- and 6-point correlations would explicitly contribute to the energy density of the thermal initial state.

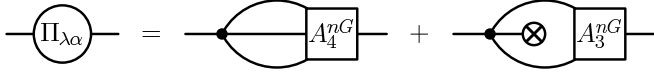


FIG. 8: Contribution  $\Pi_{\lambda\alpha}(x, y)$  to the self-energy  $\Pi(x, y)$  where the left line is connected to a classical vertex, and the right line to an effective non-local vertex.

## VII. CONCLUSIONS AND OUTLOOK

In this work, we develop techniques that allow to access vacuum and thermal equilibrium as special cases within nonequilibrium quantum field theory, which requires to take non-Gaussian initial correlations into account.

We derive Kadanoff-Baym equations for non-Gaussian correlated initial states describing vacuum and thermal equilibrium and provide suitable techniques to establish approximations to the exact thermal initial correlation functions which match the approximation scheme underlying the Kadanoff-Baym equations. These techniques are applicable for arbitrary truncations of the 2PI effective action. Examples are given for the 2PI three-loop approximation.

Finally, we discuss numerical solutions of Kadanoff-Baym equations for a real scalar  $\Phi^4$  quantum field theory, which take the thermal initial 4-point correlation as the leading non-Gaussian correction into account. These solutions are compared to solutions obtained for Gaussian initial states. For the latter, the initial state has no correlation energy by definition. Therefore, even if one initializes the two-point function with the thermal propagator for a certain temperature, the system equilibrates at a different temperature [22]. We show numerically and analytically that this feature of the Gaussian initial state is remedied completely already by taking the thermal initial 4-point correlation into account. The reason is that higher correlations of the initial state do not contribute to the total energy at the initial time. Thus, we find that including an initial 4-point correlation function yields a significantly improved approximation to the complete thermal initial state as compared to Gaussian initial states.

The techniques developed in this work provide a framework for investigating the renormalization of Kadanoff-Baym equations. It is known that the 2PI effective action can be renormalized in thermal equilibrium [28, 29]. Accordingly, it is possible to derive renormalized Kadanoff-Baym equations for the thermal initial state using the techniques introduced above. These provide a well-defined *expansion point* for nonequilibrium initial states. For example, it is possible to parameterize the initial  $n$ -point correlation functions in the form  $\alpha_n = \alpha_n^{th} + \Delta\alpha_n$ . In the limit  $\Delta\alpha_n \rightarrow 0$ , the thermal initial state is recovered and thus the Kadanoff-Baym equations are formally finite. Then it is possible to investigate which conditions the deviations  $\Delta\alpha_n$  have to fulfill such that no new divergences are introduced. This is left to future work.

## Acknowledgments

The numerical solutions were obtained on the HLRB II (SGI Altix 4700) at the Leibniz Supercomputing Centre. We thank Jürgen Berges, Szabolcs Borsanyi, Guy Moore, Emil Mottola and Urko Reinosa for helpful comments and discussions.

## APPENDIX A: PERTURBATIVE CALCULATION OF THERMAL DENSITY MATRIX ELEMENT

In order to describe the equilibrium limit within non-equilibrium quantum field theory, it is important to calculate the thermal density matrix element  $\langle \varphi_+ | \rho_{th} | \varphi_- \rangle$  evaluated with respect to two eigenstates  $\Phi(0, \mathbf{x}) | \varphi_{\pm} \rangle = \varphi_{\pm}(\mathbf{x}) | \varphi_{\pm} \rangle$  of the field operator  $\Phi(t, \mathbf{x})$  at time  $t = t_{init} \equiv 0$ . In the following, the perturbative expansion of the thermal density matrix element is discussed based on Ref. [38]. Therefore, the action (1) is formulated on the imaginary time path, and split into the free part  $S_0[\phi_0] = \int_{\mathcal{I}} d^4x ((\partial\phi_0)^2 - m^2\phi_0^2)/2$  and the interaction part  $S_{int}[\phi] = -\int_{\mathcal{I}} d^4x \frac{\lambda}{4!} \phi(x)^4$ . For the free thermal density matrix  $\rho_0 = \frac{1}{Z_0} \exp(-\beta H_0)$  containing the free Hamiltonian  $H_0$ , which is quadratic in the field, the matrix element can be calculated by a path integral that is analogous to eq. (21). The result is [38]

$$\langle \varphi_+ | \rho_0 | \varphi_- \rangle = \mathcal{N}_0 \exp \left[ iS_0[\phi_0] \right],$$

where  $\mathcal{N}_0$  is a normalization factor, which is independent of  $\varphi_{\pm}$ , and  $\phi_0(x)$  is the solution of the free equation of motion  $\delta S_0/\delta\phi = (-\square - m^2)\phi_0 = 0$  on  $\mathcal{I}$  subject to the boundary conditions

$$\phi_0(0, \mathbf{x}) = \varphi_-(\mathbf{x}) \quad \text{and} \quad \phi_0(-i\beta, \mathbf{x}) = \varphi_+(\mathbf{x}).$$

The solution is uniquely determined, and, in spatial momentum space, given by

$$\phi_0(-i\tau, \mathbf{k}) = \frac{\sinh(\omega_{\mathbf{k}}\tau)}{\sinh(\omega_{\mathbf{k}}\beta)} \varphi_+(\mathbf{k}) + \frac{\sinh(\omega_{\mathbf{k}}(\beta - \tau))}{\sinh(\omega_{\mathbf{k}}\beta)} \varphi_-(\mathbf{k}),$$

where  $\omega_{\mathbf{k}}^2 = m^2 + \mathbf{k}^2$ .

The full thermal initial correlations can be obtained by perturbing the full Hamiltonian  $H$  around  $H_0$ ,

$$\langle \varphi_+ | \rho_{th} | \varphi_- \rangle = \mathcal{N} \exp \left[ i(S_0[\phi_0] + F_{int}[\phi_0]) \right],$$

where  $\mathcal{N}$  is a normalization factor and  $iS_0[\phi_0]$  is the free contribution.  $iF_{int}[\phi_0]$  is the sum of all connected Feynman diagrams with vertices given by the derivatives of  $S_{int}[\phi]$  evaluated for  $\phi(x) = 0$ ,

$$\frac{i\delta^4 S_{int}}{\delta\phi^4} = -i\lambda\delta_{\mathcal{I}}(x_1 - x_2)\delta_{\mathcal{I}}(x_1 - x_3)\delta_{\mathcal{I}}(x_1 - x_4) = \text{diagram with four external lines meeting at a central vertex with a cross inside}.$$

According to the Feynman rules given in section III the empty circle reminds us that the corresponding integration runs over the imaginary-time contour  $\mathcal{I}$ . The boundary conditions of the path integral (21) are formally taken into account by the ‘‘field expectation value’’

$$\phi_0(-i\tau, \mathbf{k}) = \dots\dots\dots \otimes,$$

along the imaginary contour  $\mathcal{I}$ , as well as the propagator

$$\begin{aligned} D_0(-i\tau, -i\tau', \mathbf{k}) &= \dots\dots\dots \quad (\text{A1}) \\ &= \frac{1}{\omega_{\mathbf{k}} \sinh(\omega_{\mathbf{k}}\beta)} \left( \sinh(\omega_{\mathbf{k}}\tau) \sinh(\omega_{\mathbf{k}}(\beta - \tau')) \Theta(\tau' - \tau) \right. \\ &\quad \left. + \sinh(\omega_{\mathbf{k}}\tau') \sinh(\omega_{\mathbf{k}}(\beta - \tau)) \Theta(\tau - \tau') \right), \end{aligned}$$

which is the Greens function for solutions of the free equation of motion that vanish at the boundaries  $\tau = 0, \beta$ .  $D_0$  is denoted by the dotted line. To first order in  $\lambda$ ,  $iF_{int}[\phi_0]$  is given by

$$\begin{aligned} iF_{int}[\phi_0]|_{\mathcal{O}(\lambda)} &= \text{diagram 1} + \text{diagram 2} + \text{diagram 3} \\ &= \frac{-i\lambda}{4!} \int_{\mathcal{I}} d^4x \left[ 3D_0^2(x, x) + 6\phi_0^2(x)D_0(x, x) + \phi_0^4(x) \right]. \end{aligned}$$

The field-independent diagrams, like the first one above, can be absorbed into the normalization  $\mathcal{N}$ . The perturbative expansions of the thermal initial correlations  $\alpha_n^{th}$  are obtained by the  $n$ -th functional derivative of  $F[\varphi_+, \varphi_-] \equiv S_0[\phi_0] + F_{int}[\phi_0]$  with respect to the field,

$$i\alpha_n^{th, \epsilon_1, \dots, \epsilon_n}(\mathbf{x}_1, \dots, \mathbf{x}_n) = \frac{\delta iF[\varphi_+, \varphi_-]}{\delta \varphi_{\epsilon_1}(\mathbf{x}_1) \dots \delta \varphi_{\epsilon_n}(\mathbf{x}_n)} \Big|_{\varphi=0},$$

to which all diagrams with  $n$  insertions of  $\phi_0$  contribute. Here, the decomposition from eq. (9) has been used. Thus, the initial correlations obtained in this way are indeed supported only at the initial time, as required. Formally, the functional derivative corresponds to replacing the field insertions by (distinguishable) external lines in the diagrammatic expansion of  $iF_{int}[\phi_0]$  according to

$$\begin{aligned} \phi_0(-i\tau, \mathbf{k}) &\mapsto \Delta_0(-i\tau, x^0, \mathbf{k}) \\ \dots\dots\dots \otimes &\mapsto \dots\dots\dots | \text{---} , \end{aligned}$$

where  $\Delta_0(-i\tau, x^0, \mathbf{k})$  is defined in eq. (24). For example, the leading contribution to the thermal initial four-point correlation function obtained from the fourth derivative of  $iF_{int}[\phi_0]$  is given by (see eq. (26))

$$\begin{aligned} i\alpha_{4,0L}^{th}(x_1, x_2, x_3, x_4) &= \text{diagram 4} \quad (\text{A2}) \\ &= -i\lambda \int_{\mathcal{I}} d^4v \Delta_0(v, x_1) \Delta_0(v, x_2) \Delta_0(v, x_3) \Delta_0(v, x_4). \end{aligned}$$

Switching again to momentum space, an explicit expression for the leading contribution to the perturbative thermal initial four-point correlation function is obtained,

$$\begin{aligned} i\alpha_{4,0L}^{th, \epsilon_1, \epsilon_2, \epsilon_3, \epsilon_4}(\mathbf{k}_1, \mathbf{k}_2, \mathbf{k}_3, \mathbf{k}_4) &= -\lambda \int_0^\beta d\tau \Delta_0^{\epsilon_1}(-i\tau, \mathbf{k}_1) \\ &\quad \times \Delta_0^{\epsilon_2}(-i\tau, \mathbf{k}_2) \Delta_0^{\epsilon_3}(-i\tau, \mathbf{k}_3) \Delta_0^{\epsilon_4}(-i\tau, \mathbf{k}_4), \end{aligned}$$

where

$$\begin{aligned} \Delta_0^+(-i\tau, \mathbf{k}) &= \frac{\sinh(\omega_{\mathbf{k}}\tau)}{\sinh(\omega_{\mathbf{k}}\beta)}, \\ \Delta_0^-(-i\tau, \mathbf{k}) &= \frac{\sinh(\omega_{\mathbf{k}}(\beta - \tau))}{\sinh(\omega_{\mathbf{k}}\beta)}. \end{aligned}$$

The integral over the imaginary time can be performed analytically. In the zero-temperature limit ( $\beta \rightarrow \infty$ ), one obtains

$$\begin{aligned} i\alpha_{4,0L}^{th, \epsilon_1, \epsilon_2, \epsilon_3, \epsilon_4}(\mathbf{k}_1, \mathbf{k}_2, \mathbf{k}_3, \mathbf{k}_4) &\quad (\text{A3}) \\ &= \begin{cases} \frac{-\lambda}{\omega_{\mathbf{k}_1} + \omega_{\mathbf{k}_2} + \omega_{\mathbf{k}_3} + \omega_{\mathbf{k}_4}} & \text{for } \epsilon_1 = \epsilon_2 = \epsilon_3 = \epsilon_4 = \pm, \\ 0 & \text{else.} \end{cases} \end{aligned}$$

Altogether, a diagrammatic expansion of the matrix element of the thermal density matrix in terms of perturbative Feynman diagrams has been developed as suggested in Ref. [38]. This allows to explicitly calculate thermal correlation functions order by order in the quartic coupling constant. The lowest-order perturbative result (A2) may be compared to the nonperturbative 2PI result (34).

## APPENDIX B: DERIVATION OF THE CONNECTION IN THE 2PI CASE

In this appendix, we generalize eq. (23) to the 2PI formalism. Before we consider the complete thermal propagator, we find it helpful to take an intermediate step by first considering a *mixed* thermal propagator which is identical to the complete thermal propagator on the imaginary branch of the thermal time contour, and which obeys the free equation of motion on the real branches.

### 1. Mixed thermal propagator

It is straightforward to define projectors on the parts  $\mathcal{C}$  and  $\mathcal{I}$  of the thermal time contour,

$$\mathbf{1}_{\mathcal{I}}(x^0) = \begin{cases} 0 & \text{if } x^0 \in \mathcal{C} \\ 1 & \text{if } x^0 \in \mathcal{I} \end{cases}$$

and

$$\mathbf{1}_{\mathcal{C}}(x^0) = \begin{cases} 1 & \text{if } x^0 \in \mathcal{C} \\ 0 & \text{if } x^0 \in \mathcal{I} \end{cases}.$$

Of course, they fulfill the relation

$$\mathbf{1}_{\mathcal{I}}(x^0) + \mathbf{1}_{\mathcal{C}}(x^0) = 1 \quad \text{for all } x^0 \in \mathcal{C} + \mathcal{I} .$$

The mixed thermal propagator is defined by the following equation of motion,

$$G_{m,th}^{-1}(x, y) = i(\square_x + m^2)\delta_{\mathcal{C}+\mathcal{I}}(x - y) - \mathbf{1}_{\mathcal{I}}(x^0)\mathbf{1}_{\mathcal{I}}(y^0)\Pi_{th}(x, y), \quad (\text{B1})$$

where  $x^0, y^0 \in \mathcal{C} + \mathcal{I}$ . Here  $\Pi_{th}(x, y)$  is the complete thermal self-energy. The mixed propagator can be decomposed into statistical and spectral components,

$$G_{m,th}(x, y) = G_{m,F}(x, y) - \frac{i}{2}\text{sign}_{\mathcal{C}+\mathcal{I}}(x^0 - y^0)G_{m,\rho}(x, y).$$

The equation of motion for the mixed propagator can equivalently be written as

$$(\square_x + m^2)G_{m,th}(x, y) = -i\delta_{\mathcal{C}+\mathcal{I}}(x - y) - i\mathbf{1}_{\mathcal{I}}(x^0) \int_{\mathcal{I}} d^4z \Pi_{m,th}(x, z)G_{m,th}(z, y).$$

Each of the two time arguments of the propagator can either be real or imaginary, which yields four combinations  $G_{m,th}^{\mathcal{C}\mathcal{C}}, G_{m,th}^{\mathcal{C}\mathcal{I}}, G_{m,th}^{\mathcal{I}\mathcal{C}}, G_{m,th}^{\mathcal{I}\mathcal{I}}$ . The mixed propagator evaluated with two imaginary time arguments is identical to the complete thermal 2PI propagator,

$$G_{m,th}^{\mathcal{I}\mathcal{I}}(x, y) = G_{th}^{\mathcal{I}\mathcal{I}}(x, y) \quad \text{for } x^0, y^0 \in \mathcal{I}, \quad (\text{B2})$$

whereas the mixed propagators evaluated with one or two real time arguments,  $G_{m,th}^{\mathcal{C}\mathcal{I}}$  and  $G_{m,th}^{\mathcal{C}\mathcal{C}}$ , fulfill the equation of motion of the free propagator,

$$\begin{aligned} (\square_x + m^2)G_{m,th}^{\mathcal{C}\mathcal{I}}(x, y) &= 0, \\ (\square_x + m^2)G_{m,F}^{\mathcal{C}\mathcal{C}}(x, y) &= (\square_x + m^2)G_{m,\rho}^{\mathcal{C}\mathcal{C}}(x, y) = 0. \end{aligned} \quad (\text{B3})$$

At the initial time  $x^0 = y^0 = 0$ , the propagators on all branches of the thermal time path agree. Using eq. (B2), one obtains

$$G_{m,th}^{\mathcal{P}_1\mathcal{P}_2}(x, y)|_{x^0=y^0=0} = G_{th}(x, y)|_{x^0=y^0=0},$$

for  $\mathcal{P}_i \in \{\mathcal{C}, \mathcal{I}\}$ . Thus, the initial value of the mixed propagator at  $x^0 = y^0 = 0$  is given by the complete thermal propagator.

For the mixed propagator with one imaginary and one real time, the equation of motion, transformed to spatial momentum space, reads

$$\begin{aligned} (-\partial_\tau^2 + \mathbf{k}^2 + m^2)G_{m,th}^{\mathcal{I}\mathcal{C}}(-i\tau, y^0, \mathbf{k}) \\ = - \int_0^\beta d\tau' \Pi_{th}^{\mathcal{I}\mathcal{I}}(-i\tau, -i\tau', \mathbf{k})G_{m,th}^{\mathcal{I}\mathcal{C}}(-i\tau', y^0, \mathbf{k}). \end{aligned}$$

Next, a Fourier transformation with respect to the imaginary time is performed, using in particular

$$\begin{aligned} \int_0^\beta d\tau \exp(-i\omega_n\tau) \partial_\tau^2 G_{m,th}^{\mathcal{I}\mathcal{C}}(-i\tau, y^0, \mathbf{k}) \\ = -\omega_n^2 G_{m,th}^{\mathcal{I}\mathcal{C}}(\omega_n, y^0, \mathbf{k}) \\ + \text{disc}(i\omega_n G_{m,th}^{\mathcal{I}\mathcal{C}} + \partial_\tau G_{m,th}^{\mathcal{I}\mathcal{C}})(y^0, \mathbf{k}), \end{aligned}$$

where  $\omega_n = 2\pi\beta n$  is a Matsubara frequency. It is important to take the contribution from boundary terms into account,

$$\begin{aligned} \text{disc}(i\omega_n G_{m,th}^{\mathcal{I}\mathcal{C}} + \partial_\tau G_{m,th}^{\mathcal{I}\mathcal{C}})(y^0, \mathbf{k}) \\ = \left[ (i\omega_n G_{m,th}^{\mathcal{I}\mathcal{C}} + \partial_\tau G_{m,th}^{\mathcal{I}\mathcal{C}})(-i\tau, y^0, \mathbf{k}) \right]_{\tau=0}^{\tau=\beta}. \end{aligned}$$

Thus, the Fourier transformed equation for the mixed propagator reads

$$\begin{aligned} (\omega_n^2 + \mathbf{k}^2 + m^2)G_{m,th}^{\mathcal{I}\mathcal{C}}(\omega_n, y^0, \mathbf{k}) \\ = -\Pi_{th}^{\mathcal{I}\mathcal{I}}(\omega_n, \mathbf{k})G_{m,th}^{\mathcal{I}\mathcal{C}}(\omega_n, y^0, \mathbf{k}) \\ + \text{disc}(i\omega_n G_{m,th}^{\mathcal{I}\mathcal{C}} + \partial_\tau G_{m,th}^{\mathcal{I}\mathcal{C}})(y^0, \mathbf{k}). \end{aligned} \quad (\text{B4})$$

The boundary terms have to fulfill the equation of motion

$$\begin{aligned} (\partial_{y^0}^2 + \mathbf{k}^2 + m^2) \text{disc}(G_{m,th}^{\mathcal{I}\mathcal{C}})(y^0, \mathbf{k}) &= 0, \\ (\partial_{y^0}^2 + \mathbf{k}^2 + m^2) \text{disc}(\partial_\tau G_{m,th}^{\mathcal{I}\mathcal{C}})(y^0, \mathbf{k}) &= 0, \end{aligned}$$

which follows using  $G_{m,th}^{\mathcal{I}\mathcal{C}}(\omega_n, y^0, \mathbf{k}) = G_{m,th}^{\mathcal{C}\mathcal{I}}(y^0, \omega_n, \mathbf{k})$  and the equation of motion (B3) for  $G_{m,th}^{\mathcal{C}\mathcal{I}}$ . Furthermore, the initial conditions at  $y^0 = 0$  are fixed by the periodicity relation of the thermal propagator as well as the equal-time commutation relations,

$$\begin{aligned} \text{disc}(G_{m,th}^{\mathcal{I}\mathcal{C}})(0, \mathbf{k}) &= 0, \\ \partial_{y^0} \text{disc}(G_{m,th}^{\mathcal{I}\mathcal{C}})(0, \mathbf{k}) &= i, \\ \text{disc}(\partial_\tau G_{m,th}^{\mathcal{I}\mathcal{C}})(0, \mathbf{k}) &= 1, \\ \partial_{y^0} \text{disc}(\partial_\tau G_{m,th}^{\mathcal{I}\mathcal{C}})(0, \mathbf{k}) &= 0. \end{aligned}$$

The statistical and spectral components  $G_{m,F}^{\mathcal{C}\mathcal{C}}(0, y^0, \mathbf{k})$  and  $G_{m,\rho}^{\mathcal{C}\mathcal{C}}(0, y^0, \mathbf{k})$  of the mixed propagator are two linearly independent solutions of the free equation of motion. Since it is a second order differential equation, any solution can be expressed as a linear combination, especially

$$\begin{aligned} \text{disc}(G_{m,th}^{\mathcal{I}\mathcal{C}})(y^0, \mathbf{k}) &= -iG_{m,\rho}^{\mathcal{C}\mathcal{C}}(0, y^0, \mathbf{k}), \\ \text{disc}(\partial_\tau G_{m,th}^{\mathcal{I}\mathcal{C}})(y^0, \mathbf{k}) &= \frac{G_{m,F}^{\mathcal{C}\mathcal{C}}(0, y^0, \mathbf{k})}{G_{th}(0, 0, \mathbf{k})}. \end{aligned}$$

Inserting this result into eq. (B4) and using the Fourier-transformed Schwinger-Dyson equation (29) for the complete thermal propagator yields

$$\begin{aligned} G_{m,th}^{\mathcal{I}\mathcal{C}}(\omega_n, y^0, \mathbf{k}) &= \left( \frac{G_{th}^{\mathcal{I}\mathcal{I}}(\omega_n, \mathbf{k})}{G_{th}(0, 0, \mathbf{k})} \right) G_{m,F}^{\mathcal{C}\mathcal{C}}(0, y^0, \mathbf{k}) \\ &\quad - (i\omega_n G_{th}^{\mathcal{I}\mathcal{I}}(\omega_n, \mathbf{k})) G_{m,\rho}^{\mathcal{C}\mathcal{C}}(0, y^0, \mathbf{k}). \end{aligned}$$

Finally, the upper relation can be rewritten in the form

$$G_{m,th}^{\mathcal{I}\mathcal{C}}(\omega_n, y^0, \mathbf{k}) = \int_{\mathcal{C}} dz^0 \Delta_m(\omega_n, z^0, \mathbf{k}) G_{m,th}^{\mathcal{C}\mathcal{C}}(z^0, y^0, \mathbf{k}), \quad (\text{B5})$$

where a *mixed connection* has been introduced,

$$\begin{aligned} \Delta_m(\omega_n, z^0, \mathbf{k}) &= \Delta_m^s(\omega_n, \mathbf{k}) \delta_s(z^0) + \Delta_m^a(\omega_n, \mathbf{k}) \delta_a(z^0) \\ &= \left( \frac{G_{th}^{\mathcal{I}\mathcal{I}}(\omega_n, \mathbf{k})}{G_{th}(0, 0, \mathbf{k})} \right) \delta_s(z^0) + \left( 2i\omega_n G_{th}^{\mathcal{I}\mathcal{I}}(\omega_n, \mathbf{k}) \right) \delta_a(z^0) \\ &= \text{-----} | \text{---} . \end{aligned} \quad (\text{B6})$$

Furthermore, the transposed connection is defined as  $\Delta_m^T(z^0, \omega_n, \mathbf{k}) = \Delta_m(\omega_n, z^0, \mathbf{k})$ . Eq. (B5) for the mixed propagator is the generalization of eq. (23) for the free propagator. Thus, the mixed propagator evaluated with one real and one imaginary time can be written as the convolution of the mixed connection, which involves the complete 2PI propagator, and the real-real mixed propagator, which obeys the free equation of motion.

## 2. Complete thermal propagator

Using the equation of motion (B1) of the mixed propagator, the self-consistent equation of motion (29) of the complete propagator can be rewritten as

$$G_{th}^{-1}(x, y) = G_{m,th}^{-1}(x, y) - [1 - \mathbf{1}_{\mathcal{I}}(x^0) \mathbf{1}_{\mathcal{I}}(y^0)] \Pi_{th}(x, y),$$

for  $x^0, y^0 \in \mathcal{C} + \mathcal{I}$ . By convolving this equation with  $G_{th}$  from the left and with  $G_{m,th}$  from the right, the integral form of the Schwinger-Dyson equation is obtained:

$$G_{th}(x, y) = G_{m,th}(x, y) + \int_{\mathcal{C} + \mathcal{I}} d^4u \int_{\mathcal{C} + \mathcal{I}} d^4v G_{th}(x, u) \times [1 - \mathbf{1}_{\mathcal{I}}(u^0) \mathbf{1}_{\mathcal{I}}(v^0)] \Pi_{th}(u, v) G_{m,th}(v, y). \quad (\text{B7})$$

Evaluating it for  $x^0 \in \mathcal{C}$  and  $y^0 \in \mathcal{I}$ , and performing a Fourier transformation with respect to the relative spatial coordinate  $\mathbf{x} - \mathbf{y}$  as well as the imaginary time  $y^0$  gives

$$\begin{aligned} G_{th}^{\mathcal{C}\mathcal{I}}(x^0, \omega_n, \mathbf{k}) &= G_{m,th}^{\mathcal{C}\mathcal{I}}(x^0, \omega_n, \mathbf{k}) \\ &+ \int_{\mathcal{C} + \mathcal{I}} du^0 \int_{\mathcal{C}} dv^0 G_{th}(x^0, u^0, \mathbf{k}) \\ &\quad \times \Pi_{th}(u^0, v^0, \mathbf{k}) G_{m,th}^{\mathcal{C}\mathcal{I}}(v^0, \omega_n, \mathbf{k}) \\ &- i \int_{\mathcal{C}} du^0 G_{th}^{\mathcal{C}\mathcal{C}}(x^0, u^0, \mathbf{k}) \Pi_{th}(u^0, \omega_n, \mathbf{k}) G_{m,th}^{\mathcal{I}\mathcal{I}}(\omega_n, \mathbf{k}). \end{aligned}$$

Next,  $G_{m,th}^{\mathcal{C}\mathcal{I}}(x^0, \omega_n, \mathbf{k})$  and  $G_{m,th}^{\mathcal{C}\mathcal{I}}(v^0, \omega_n, \mathbf{k})$  are replaced using eq. (B5) with interchanged arguments. Furthermore, it is used that  $G_{m,th}^{\mathcal{I}\mathcal{I}}(\omega_n, \mathbf{k}) = G_{th}^{\mathcal{I}\mathcal{I}}(\omega_n, \mathbf{k})$  (see eq. (B2)):

$$\begin{aligned} G_{th}^{\mathcal{C}\mathcal{I}}(x^0, \omega_n, \mathbf{k}) &= \int_{\mathcal{C}} dz^0 G_{m,th}^{\mathcal{C}\mathcal{C}}(x^0, z^0, \mathbf{k}) \Delta_m^T(z^0, \omega_n, \mathbf{k}) \\ &+ \int_{\mathcal{C}} dz^0 \int_{\mathcal{C} + \mathcal{I}} du^0 \int_{\mathcal{C}} dv^0 G_{th}(x^0, u^0, \mathbf{k}) \Pi_{th}(u^0, v^0, \mathbf{k}) G_{m,th}^{\mathcal{C}\mathcal{C}}(v^0, z^0, \mathbf{k}) \Delta_m^T(z^0, \omega_n, \mathbf{k}) \\ &- i \int_{\mathcal{C}} du^0 G_{th}^{\mathcal{C}\mathcal{C}}(x^0, u^0, \mathbf{k}) \Pi_{th}(u^0, \omega_n, \mathbf{k}) G_{th}^{\mathcal{I}\mathcal{I}}(\omega_n, \mathbf{k}) \\ &= \int_{\mathcal{C}} dz^0 \left[ G_{th}^{\mathcal{C}\mathcal{C}}(x^0, z^0, \mathbf{k}) - \int_{\mathcal{C}} du^0 \int_{\mathcal{I}} dv^0 \left( G_{th}^{\mathcal{C}\mathcal{C}}(x^0, u^0, \mathbf{k}) \Pi_{th}(u^0, v^0, \mathbf{k}) G_{m,th}^{\mathcal{I}\mathcal{C}}(v^0, z^0, \mathbf{k}) \right) \right] \Delta_m^T(z^0, \omega_n, \mathbf{k}) \\ &- i \int_{\mathcal{C}} du^0 G_{th}^{\mathcal{C}\mathcal{C}}(x^0, u^0, \mathbf{k}) \Pi_{th}(u^0, \omega_n, \mathbf{k}) G_{th}^{\mathcal{I}\mathcal{I}}(\omega_n, \mathbf{k}) \\ &= \int_{\mathcal{C}} dz^0 G_{th}^{\mathcal{C}\mathcal{C}}(x^0, z^0, \mathbf{k}) \left\{ \Delta_m^T(z^0, \omega_n, \mathbf{k}) - i \Pi_{th}(z^0, \omega_n, \mathbf{k}) G_{th}^{\mathcal{I}\mathcal{I}}(\omega_n, \mathbf{k}) \right. \\ &\quad \left. - \int_{\mathcal{C}} du^0 \int_{\mathcal{I}} dv^0 \Pi_{th}(z^0, v^0, \mathbf{k}) G_{m,th}^{\mathcal{I}\mathcal{C}}(v^0, u^0, \mathbf{k}) \Delta_m^T(u^0, \omega_n, \mathbf{k}) \right\}. \end{aligned}$$

In the second step, the Schwinger-Dyson equation (B7) evaluated for  $x^0, z^0 \in \mathcal{C}$  was used again. In the third

step the complete real-real propagator was factored out

by interchanging the integration variables  $u^0 \leftrightarrow z^0$  in the second and third term. The last line can be simplified by Fourier transforming with respect to the imaginary time  $v^0$ , and performing the integral over  $\mathcal{C}$  using eq. (B6):

$$\begin{aligned} & \int_{\mathcal{C}} du^0 \int_{\mathcal{I}} dv^0 \Pi_{th}(z^0, v^0, \mathbf{k}) G_{m,th}^{\mathcal{I}\mathcal{C}}(v^0, u^0, \mathbf{k}) \Delta_m^T(u^0, \omega_n, \mathbf{k}) \\ &= -iT \sum_l \Pi_{th}(z^0, \omega_l, \mathbf{k}) G_{m,th}^{\mathcal{I}\mathcal{C}}(\omega_l, 0, \mathbf{k}) \Delta_m^s(\omega_n, \mathbf{k}) \\ &= -iT \sum_l \Pi_{th}(z^0, \omega_l, \mathbf{k}) G_{th}^{\mathcal{I}\mathcal{I}}(\omega_l, \mathbf{k}) \frac{G_{th}^{\mathcal{I}\mathcal{I}}(\omega_n, \mathbf{k})}{G_{th}(0, 0, \mathbf{k})}. \end{aligned}$$

Finally, a decomposition of the complete thermal 2PI propagator evaluated with one real time and one Matsubara frequency is obtained,

$$G_{th}^{\mathcal{C}\mathcal{I}}(x^0, \omega_n, \mathbf{k}) = \int_{\mathcal{C}} dz^0 G_{th}^{\mathcal{C}\mathcal{C}}(x^0, z^0, \mathbf{k}) \Delta^T(z^0, \omega_n, \mathbf{k}),$$

where the *complete connection* was introduced,

$$\begin{aligned} \Delta^T(z^0, \omega_n, \mathbf{k}) &= \Delta_m^T(z^0, \omega_n, \mathbf{k}) \\ &- iT \sum_m \Pi_{th}(z^0, \omega_m, \mathbf{k}) D(\omega_m, \omega_n, \mathbf{k}), \end{aligned} \quad (\text{B8})$$

with  $\Delta(\omega_n, z^0, \mathbf{k}) = \Delta^T(z^0, \omega_n, \mathbf{k})$ . Compared to the mixed connection, the complete connection contains an additional term, which is the convolution of the thermal self-energy, evaluated with one real time and one Matsubara frequency, with the propagator  $D(\omega_m, \omega_n, \mathbf{k})$ . This propagator is given by

$$\begin{aligned} D(\omega_n, \omega_m, \mathbf{k}) &= \frac{\delta_{n,m}}{T} G_{th}^{\mathcal{I}\mathcal{I}}(\omega_n, \mathbf{k}) \\ &- \int_{\mathcal{C}} dw^0 \int_{\mathcal{C}} dz^0 \Delta(\omega_n, w^0, \mathbf{k}) G_{th}(w^0, z^0, \mathbf{k}) \Delta^T(z^0, \omega_m, \mathbf{k}) \\ &= \frac{\delta_{n,m}}{T} G_{th}^{\mathcal{I}\mathcal{I}}(\omega_n, \mathbf{k}) - \frac{G_{th}^{\mathcal{I}\mathcal{I}}(\omega_n, \mathbf{k}) G_{th}^{\mathcal{I}\mathcal{I}}(\omega_m, \mathbf{k})}{G_{th}(0, 0, \mathbf{k})}. \end{aligned} \quad (\text{B9})$$

In the last line

$$\int_{\mathcal{C}} dw^0 \int_{\mathcal{C}} dz^0 X(\omega_n, w^0, \mathbf{k}) G_{th}(w^0, z^0, \mathbf{k}) \Pi_{th}(z^0, \omega_m, \mathbf{k}) = 0$$

was used, where  $X \in \{\Delta, \Pi_{th}\}$ . The propagator  $D$  has the properties

$$\begin{aligned} D(\omega_n, \omega_m, \mathbf{k}) &= D(\omega_m, \omega_n, \mathbf{k}), \\ T \sum_m D(\omega_n, \omega_m, \mathbf{k}) &= 0. \end{aligned}$$

From the last property it can be inferred that only the non-local part of the thermal self-energy  $\Pi_{th}(z^0, \omega_m, \mathbf{k}) = \Pi_{th}^{loc} + \Pi_{th}^{nl}(z^0, \omega_m, \mathbf{k})$  contributes in eq. (B8), since the local part is independent of the Matsubara frequency.

By applying an inverse Fourier transformation with respect to imaginary time, using in particular

$$D(-i\tau, -i\tau', \mathbf{k}) = T^2 \sum_{n,m} e^{i\omega_n \tau - i\omega_m \tau'} D(\omega_n, \omega_m, \mathbf{k}),$$

the complete thermal 2PI propagator with one imaginary and one real time can be decomposed as

$$G_{th}^{\mathcal{C}\mathcal{I}}(x^0, -i\tau, \mathbf{k}) = \int_{\mathcal{C}} dz^0 G_{th}^{\mathcal{C}\mathcal{C}}(x^0, z^0, \mathbf{k}) \Delta^T(z^0, -i\tau, \mathbf{k}),$$

$$\bullet \text{---} \circ = \bullet \text{---} | \text{---} \circ,$$

and

$$G_{th}^{\mathcal{I}\mathcal{C}}(-i\tau, y^0, \mathbf{k}) = \int_{\mathcal{C}} dz^0 \Delta(-i\tau, z^0, \mathbf{k}) G_{th}^{\mathcal{C}\mathcal{C}}(z^0, y^0, \mathbf{k}),$$

$$\circ \text{---} \bullet = \circ \text{---} | \text{---} \bullet, \quad (\text{B10})$$

where the complete connection is given by

$$\begin{aligned} \Delta(-i\tau, z^0, \mathbf{k}) &= \Delta_m(-i\tau, z^0, \mathbf{k}) \\ &+ \int_{\mathcal{I}} dv^0 D(-i\tau, v^0, \mathbf{k}) \Pi_{th}^{nl}(v^0, z^0, \mathbf{k}) \\ &= \Delta^s(-i\tau, \mathbf{k}) \delta_s(z^0) + \Delta^a(-i\tau, \mathbf{k}) \delta_a(z^0) \\ &+ \int_{\mathcal{I}} dv^0 D(-i\tau, v^0, \mathbf{k}) \Pi_{th}^{nl}(v^0, z^0, \mathbf{k}) \\ &= \text{---} | \text{---} + \text{---} \circ \Pi_{th}^{nl} \bullet \text{---} \\ &\equiv \text{---} | \text{---}, \end{aligned} \quad (\text{B11})$$

and

$$\Delta^T(z^0, -i\tau, \mathbf{k}) = \Delta(-i\tau, z^0, \mathbf{k}) = \bullet \text{---} | \text{---} \text{---}.$$

The coefficients  $\Delta^{s,a}(-i\tau, \mathbf{k})$  are given by

$$\begin{aligned} \Delta^s(-i\tau, \mathbf{k}) &= \frac{G_{th}^{\mathcal{I}\mathcal{I}}(-i\tau, 0, \mathbf{k})}{G_{th}(0, 0, \mathbf{k})}, \\ \Delta^a(-i\tau, \mathbf{k}) &= 2\partial_\tau G_{th}^{\mathcal{I}\mathcal{I}}(-i\tau, 0, \mathbf{k}). \end{aligned} \quad (\text{B12})$$

Eqs. (B10,B11,B12) constitute the nonperturbative generalizations of eqs. (23,24).

The nonperturbative generalization of eq. (28) is obtained from eq. (B9),

$$\begin{aligned} & G_{th}^{\mathcal{I}\mathcal{I}}(-i\tau, -i\tau', \mathbf{k}) \\ &= D(-i\tau, -i\tau', \mathbf{k}) + \int_{\mathcal{C}} dw^0 \int_{\mathcal{C}} dz^0 \Delta(-i\tau, w^0, \mathbf{k}) \\ &\quad \times G_{th}(w^0, z^0, \mathbf{k}) \Delta^T(z^0, -i\tau', \mathbf{k}) \\ &= D(-i\tau, -i\tau', \mathbf{k}) \\ &\quad + \Delta^s(-i\tau, \mathbf{k}) G_{th}(0, 0, \mathbf{k}) \Delta^s(-i\tau', \mathbf{k}). \end{aligned} \quad (\text{B13})$$

Note that only the parts of the connections containing  $\Delta^s$  contribute to the double integral in the second and

third line, whereas the parts involving  $\Delta^a$  and  $\Pi_{th}^{nl}$  vanish due to a cancellation of the contributions from the two branches of the closed real-time path. Using the Feynman rules from above, the upper equation can also be written as

$$\begin{aligned} \text{---} \circ \text{---} \circ \text{---} &= \text{---} \circ \text{---} \circ \text{---} + \text{---} \circ \text{---} \text{---} \text{---} \text{---} \circ \text{---} \\ &= \text{---} \circ \text{---} \circ \text{---} + \text{---} \circ \text{---} \text{---} \text{---} \text{---} \circ \text{---} . \end{aligned}$$

In Summary, there are two differences compared to the perturbative case: (i) the free thermal propaga-

tor  $G_{0,th}(-i\tau, 0, \mathbf{k})$  enters the free connection, whereas the complete thermal propagator  $G_{th}(-i\tau, 0, \mathbf{k})$  enters the complete connection, and (ii) the free connection  $\Delta_0(-i\tau, z^0, \mathbf{k})$  is only supported at the initial time  $z^0 = 0_{\pm}$ , whereas the complete connection  $\Delta(-i\tau, z^0, \mathbf{k})$  features an additional term containing the non-local part of the complete thermal self-energy.

- 
- [1] Lev Kofman, Andrei D. Linde, and Alexei A. Starobinsky, *Towards the theory of reheating after inflation*, Phys. Rev. **D56** (1997) 3258, hep-ph/9704452.
  - [2] Peter F. Kolb and Ulrich W. Heinz, *Hydrodynamic description of ultrarelativistic heavy-ion collisions* (2003), nucl-th/0305084.
  - [3] Edward W. Kolb and Michael S. Turner, *The Early universe* (1990), redwood City, USA: Addison-Wesley (1990) 547 p. (Frontiers in physics, 69)
  - [4] Eiichiro Komatsu et al. (WMAP), *Five-Year Wilkinson Microwave Anisotropy Probe (WMAP) Observations: Cosmological Interpretation*, Astrophys. J. Suppl. **180** (2009) 330, 0803.0547.
  - [5] Jürgen Berges and Jürgen Cox, *Thermalization of quantum fields from time-reversal invariant evolution equations*, Phys. Lett. **B517** (2001) 369, hep-ph/0006160.
  - [6] Jürgen Berges, *Controlled nonperturbative dynamics of quantum fields out of equilibrium*, Nucl. Phys. **A699** (2002) 847, hep-ph/0105311.
  - [7] Gert Aarts and Jürgen Berges, *Classical aspects of quantum fields far from equilibrium*, Phys. Rev. Lett. **88** (2002) 041603, hep-ph/0107129.
  - [8] Gert Aarts and Jose M. Martínez Resco, *Transport coefficients from the 2PI effective action*, Phys. Rev. **D68** (2003) 085009, hep-ph/0303216.
  - [9] Manfred Lindner and Markus Michael Müller, *Comparison of Boltzmann equations with quantum dynamics for scalar fields*, Phys. Rev. **D73** (2006) 125002, hep-ph/0512147.
  - [10] John M. Cornwall, Roman Jackiw, and Eleftherios Tomboulis, *Effective Action for Composite Operators*, Phys. Rev. **D10** (1974) 2428.
  - [11] Julian S. Schwinger, *Brownian motion of a quantum oscillator*, J. Math. Phys. **2** (1961) 407.
  - [12] Leonid V. Keldysh, *Diagram technique for nonequilibrium processes*, Sov. Phys. JETP **20** (1965) 1018.
  - [13] Pawel Danielewicz, *Quantum Theory of Nonequilibrium Processes I*, Annals Phys. **152** (1984) 239.
  - [14] Gert Aarts and Anders Tranberg, *Particle creation and warm inflation*, Phys. Lett. **B650** (2007) 65, hep-ph/0701205.
  - [15] Gert Aarts and Anders Tranberg, *Thermal effects on inflaton dynamics* (2007), arXiv:0712.1120 [hep-ph].
  - [16] Jürgen Berges and Julien Serreau, *Parametric resonance in quantum field theory*, Phys. Rev. Lett. **91** (2003) 111601, hep-ph/0208070.
  - [17] Jürgen Berges, Szabolcs Borsanyi, and Julien Serreau, *Thermalization of fermionic quantum fields*, Nucl. Phys. **B660** (2003) 51, hep-ph/0212404.
  - [18] Jürgen Berges, Szabolcs Borsanyi, and Christof Wetterich, *Prethermalization*, Phys. Rev. Lett. **93** (2004) 142002, hep-ph/0403234.
  - [19] Sascha Juchem, Wolfgang Cassing, and Carsten Greiner, *Quantum dynamics and thermalization for out-of-equilibrium phi\*\*4-theory*, Phys. Rev. **D69** (2004) 025006, hep-ph/0307353.
  - [20] Manfred Lindner and Markus Michael Müller, *Comparison of Boltzmann Kinetics with Quantum Dynamics for a Chiral Yukawa Model Far From Equilibrium*, Phys. Rev. **D77** (2008) 025027, arXiv:0710.2917.
  - [21] Pawel Danielewicz, *Quantum theory of nonequilibrium processes. II. Application to nuclear collisions*, Annals Phys. **152** (1984) 305.
  - [22] Sigurd Köhler, *Memory and correlation effects in nuclear collisions*, Phys. Rev. **C51** (1995) 3232.
  - [23] Sigurd Köhler, *Memory and correlation effects in the quantum theory of thermalization*, Phys. Rev. **E53** (1996) 3145.
  - [24] Klaus Morawetz and Sigurd Köhler, *Formation of correlations and energy-conservation at short time scales*, Eur. Phys. J. **A4** (1999) 291, nucl-th/9802082.
  - [25] Sigurd Köhler and Klaus Morawetz, *Correlations in Many-Body Systems with Two-time Green's Functions*, Phys. Rev. **C64** (2001) 024613, nucl-th/0102059.
  - [26] Anders Tranberg, *Quantum field thermalization in expanding backgrounds* (2008), arXiv:0806.3158.
  - [27] Andreas Hohenegger, Alexander Kartavtsev, and Manfred Lindner, *Deriving Boltzmann Equations from Kadanoff-Baym Equations in Curved Space-Time* (2008), arXiv:0807.4551.
  - [28] Jürgen Berges, Szabolcs Borsanyi, Urko Reinosa, and Julien Serreau, *Nonperturbative renormalization for 2PI effective action techniques*, Annals Phys. **320** (2005) 344, hep-ph/0503240.
  - [29] Jürgen Berges, Szabolcs Borsanyi, Urko Reinosa, and Julien Serreau, *Renormalized thermodynamics from the 2PI effective action*, Phys. Rev. **D71** (2005) 105004, hep-ph/0409123.
  - [30] Jean-Paul Blaizot, Edmond Iancu, and Urko Reinosa, *Renormalization of phi-derivable approximations in scalar field theories*, Nucl. Phys. **A736** (2004) 149, hep-ph/0312085.
  - [31] Hendrik van Hees and Joern Knoll, *Renormalization of self-consistent approximation schemes. II: Applications*

- to the sunset diagram, Phys. Rev. **D65** (2002) 105005, hep-ph/0111193.
- [32] Hendrik van Hees and Joern Knoll, *Renormalization in self-consistent approximations schemes at finite temperature. I: Theory*, Phys. Rev. **D65** (2002) 025010, hep-ph/0107200.
- [33] Szabolcs Borsanyi and Urko Reinosa, *Renormalised non-equilibrium quantum field theory: scalar fields* (2008), 0809.0496.
- [34] Antti J. Niemi and Gordon W. Semenoff, *Thermodynamic Calculations in Relativistic Finite Temperature Quantum Field Theories*, Nucl. Phys. **B230** (1984) 181.
- [35] Antti J. Niemi and Gordon W. Semenoff, *Finite Temperature Quantum Field Theory in Minkowski Space*, Ann. Phys. **152** (1984) 105.
- [36] Nicolaas P. Landsman and Christianus G. van Weert, *Real and Imaginary Time Field Theory at Finite Temperature and Density*, Phys. Rept. **145** (1987) 141.
- [37] Kuangchao Chou, Zhaobin Su, Bailin Hao, and Lu Yu, *Equilibrium and Nonequilibrium Formalisms Made Unified*, Phys. Rept. **118** (1985) 1.
- [38] Esteban Calzetta and Bei-Lok Hu, *Nonequilibrium quantum fields: closed time path effective action, Wigner function and Boltzmann equation*, Phys. Rev. **D37** (1988) 2878.
- [39] Mathias Garny, *Particle Physics and Dark Energy: Beyond Classical Dynamics*, Ph.D. thesis, Munich, Tech. U. (2008)